CRITICAL FIELD OF SUPERCONDUCTING ALUMINUM AS A FUNCTION OF TEMPERATURE AND PRESSURE ABOVE 0.3°K

by

Erik P. Harris

University of Illinois

Department of Physics

Urbana, Illinois

November, 1966

CRITICAL FIELD OF SUPERCONDUCTING ALUMINUM AS A FUNCTION OF PRESSURE AND TEMPERATURE ABOVE 0.3°K

by

ERIK PRESTON HARRIS

Technical Report
Prepared under Contract
with the Office of Ordinance Research, U. S. Army for
EXPERIMENTAL RESEARCH UPON SUPERCONDUCTING METALS
OOR Project No. 20014501B11B

U.S. Army Research Office (Durham) Project Number
DA-ORD-31-124-359

Dillon E. Mapother, Project Supervisor
University of Illinois, Urbana, Illinois

CRITICAL FIELD OF SUPERCONDUCTING ALUMINUM AS A FUNCTION OF PRESSURE AND TEMPERATURE ABOVE 0.3°K

Erik Preston Harris, Ph.D.
Department of Physics
University of Illinois, 1967

ABSTRACT

The critical field curve of aluminum has been measured from T_c to 0.3°K, at pressures ranging from 0 to 7200 psi. Using calorimetrically derived values for the low-temperature superconducting electronic specific heat, the data have been extrapolated to T = 0, yielding values for H_o and γ. These values and experimental results for T_c are then used to calculate the superconducting electronic entropy and the deviation of the critical field curve from parabolicity over the entire temperature range. The results show excellent agreement with previous calorimetric measurements of the thermodynamic properties of superconducting aluminum. The shape of the reduced critical field curve shows no pressure dependence over the range of pressures used. The dependence of H_o, T_c, and γ on pressure are in fair agreement with previous work by Gross and Olsen.*

---

*Gross and Olsen, Cryogenics 1, 91 (1960).

ACKNOWLEDGMENTS

The author wishes to express his appreciation for the guidance and encouragement of his advisor, Professor D. E. Mapother, during the period in which this work was performed.

He is also indebted to Messrs. D. U. Gubser, D. G. Hamblen, W. N. Hubin, D. Y. LeCorgne, D. Losee, and D. C. Montgomery for assistance in making the measurements.

Thanks are due to Mr. R. E. Harris who wrote some of the computer programs used in the data analysis and provided assistance with the use of the IBM 7094 computer facility.

The author also wishes to thank the Union Carbide Corporation for fellowship support during a portion of this work.

Finally, the author wishes to express his appreciation to his wife, Joyce, for her constant encouragement and support.

This project was supported by funds from the U. S. Army Research Office (Durham) and the Advanced Research Projects Agency of the Department of Defense.

TABLE OF CONTENTS

I. INTRODUCTION

A. Background

Superconductivity was discovered by Kamerlingh Onnes[1] in 1911 during an investigation of the electrical resistivity of mercury at low temperatures. He found that the electrical resistance of his mercury sample fell abruptly to zero as its temperature fell below about $4^{\circ}K$; hence the name superconductivity. It has since been found that a current induced in a superconducting ring will persist indefinitely without apparent decay.

Since 1911 a large number of pure metals and alloys have been found to be superconducting at low enough temperatures, and their properties have been extensively investigated. Only a few of the important experiments and calculations will be mentioned here. For a more complete review, the reader is referred elsewhere.[2,3]

The temperature below which a material becomes superconducting in zero magnetic field is called its critical temperature, T_c. If a long, needle-shaped specimen is cooled below this temperature in zero field, and then the magnetic field is increased from zero, it is found that the superconducting properties disappear abruptly at a critical field H_c. The temperature dependence of H_c is given approximately by

$$H_c \approx H_o\left(1 - T^2/T_c^2\right), \qquad (1)$$

where H_o and T_c are parameters characteristic of the material.

Meissner and Ochsenfeld[4] discovered in 1933 that the superconducting state is characterized by perfect diamagnetism. That is, the magnetic induction B becomes zero when a material goes from the normal state to the superconducting state. Upon reducing the applied field below H_c for T less than T_c the magnetic flux is completely expelled from the sample. This effect is known as the Meissner effect, and establishes the thermodynamic reversibility of the superconducting transition. For a specimen with any geometry other than that of a long needle the magnetic transition is broadened due to the distortion of the applied field by the diamagnetism of the sample. Consider an ellipsoidal sample with demagnetizing factor n placed in a magnetic field parallel to its major axis. When the applied field reaches $(1-n)H_c$, the field at the equator of the specimen is H_c. At this point the sample enters the transition region, known as the intermediate state, and flux begins to enter the sample. When the applied field reaches H_c, the flux has completely penetrated the sample, and for H greater than H_c the sample is in the normal state. Plots of magnetization versus applied field at constant temperature are shown in Figure 1. We shall not discuss the detailed nature of the intermediate state. Suffice it to say that the sample divides itself into superconducting and normal regions in such a way that the magnetic induction rises uniformly from zero to H_c as the applied field is increased from $(1-n)H_c$ to H_c.[5]

Figure 1. Magnetization curves for a long cylindrical superconductor and for an ellipsoidal superconductor with a demagnetization factor of 0.25.

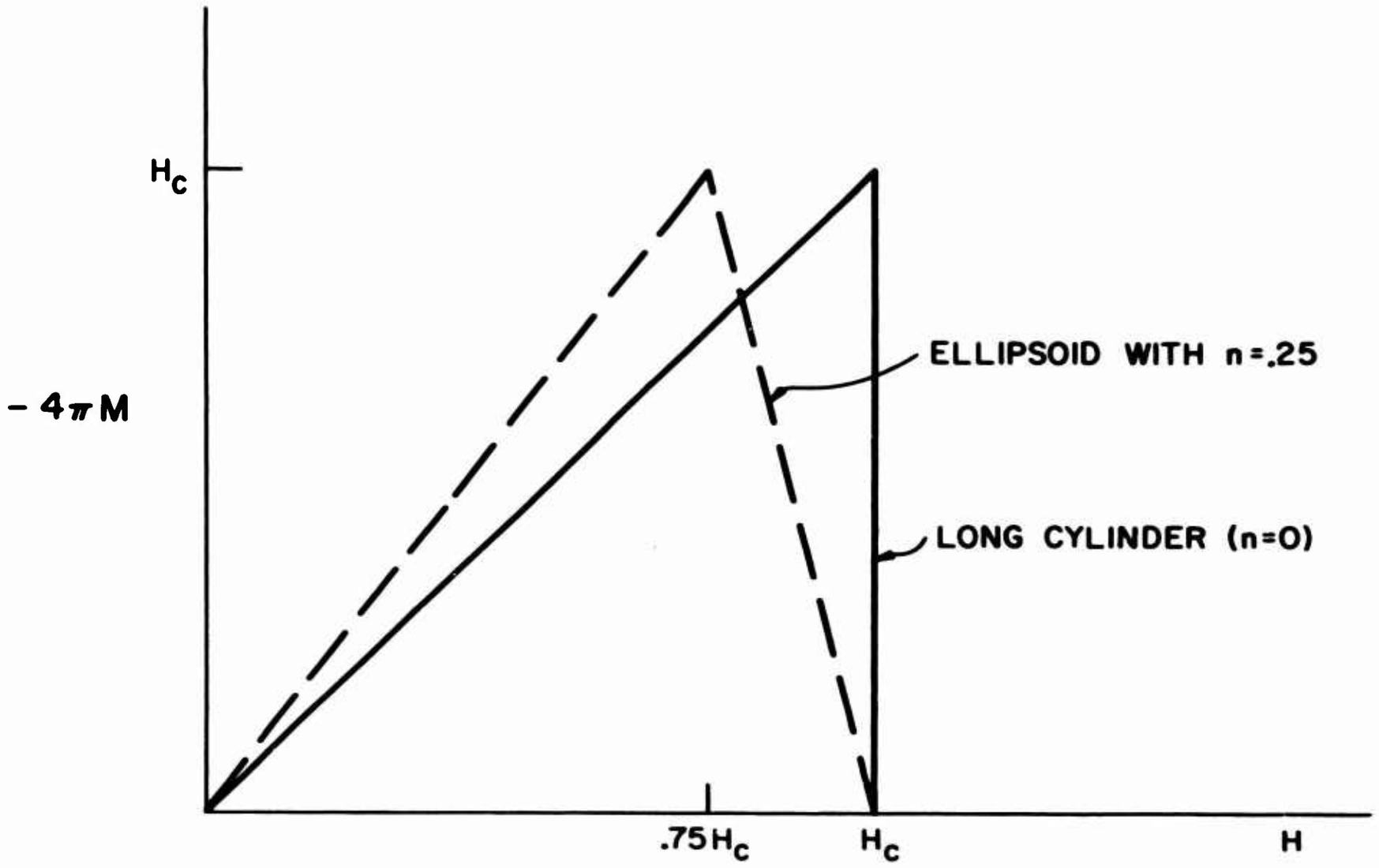
H_c
$-4\pi M$
ELLIPSOID WITH n=.25
LONG CYLINDER (n=0)
$.75H_c$
H_c
H

In recent years it has been recognized that superconductors may be grouped into two classes called Type I and Type II. The behavior just described applies to Type I superconductors, a class which includes most of the pure elemental soft metals such as Sn, In, Hg, and Aℓ. Type II materials are usually (but not invariably) alloys whose most prominent characteristics include the ability to sustain loss-less supercurrents at much larger fields than Type I metals. Type II superconductors also show marked differences in the behavior of their magnetic transitions from that described above.[3] Since the present work is exclusively concerned with Aℓ, a Type I material, we shall not review the extensive phenomenology of Type II superconductors.

Existence of the Meissner effect implies that the superconducting transition is reversible and thus susceptible to thermodynamic analysis. In the next section we will show that

$$\Delta S = -\frac{V}{4\pi} H_c \left(\frac{\partial H_c}{\partial T}\right)_P \qquad (2)$$

where ΔS is the entropy difference between the normal and superconducting states. The existence of only minute changes in elastic constants[6,7] in the superconducting transition indicates that the lattice entropy is virtually unaffected by the transition, and that the superconducting phenomenon is due to an electronic interaction.

The nature of the electronic interaction responsible for superconductivity was illuminated by the discovery of the isotope effect[8,9] in 1950. It was shown experimentally that T_c for different isotopes of mercury varied as the inverse square root of the isotopic mass, indicating that lattice vibrations play an important role in the interaction between electrons which leads to superconductivity. Since 1950 experiments have shown that the isotopic mass dependence of the critical temperature varies from material to material, and is non-existent in some materials, such as ruthenium.[10,11] However, Garland[12] has been able to account for these variations by a detailed consideration of the effects of the Coulomb interaction between electrons, without discarding the idea that superconductivity is due to an electron-phonon interaction. Further information about the superconducting state was gained from measurements of thermal conductivity[13] and the electronic specific heat in the superconducting state.[14] These measurements suggested the existence of an energy gap in the spectrum of allowed electronic excitations of a superconductor.

In 1957, Bardeen, Cooper, and Schrieffer[15] published a theory of superconductivity (hereafter referred to as the BCS theory) from which properties of superconductors can be calculated. The BCS theory predictions for the temperature dependence of the energy gap, for instance, are in good agreement with direct measurements.[16] Such measurements are made by measuring the absorption of electromagnetic radiation as a function of frequency or by measuring

electron tunneling between a superconductor and another metal through an insulating barrier. Experimental values of the gap extrapolated to $0^{\circ}K$, however, vary from material to material and differ from the BCS value by as much as 30 or 40%.

The BCS theory, using a simplified model of the electron-electron interaction via phonons, and ignoring the details of crystal structure which vary from metal to metal, predicts a law of corresponding states. For instance, the critical field curve in terms of the reduced quantities H_c/H_o and T/T_c is predicted to have the same shape for all superconductors. Experiments have shown that in fact deviations of H_c/H_o from a law of corresponding states are in general only a few percent.[17] These deviations can be accurately measured, however, and are useful for comparison with theory. The largest deviations from the BCS law of corresponding states have been observed in lead and mercury, so-called strong-coupling superconductors. Recent theoretical calculations of strong-coupling effects by Swihart and others[18] have improved agreement between theory and experiment for the strong-coupling superconductors. Critical field data of sufficient quality to permit such a comparison with theory exist for many superconductors with critical temperatures well above $1^{\circ}K$, but for most low-temperature superconductors, such as aluminum, such data do not exist.

This thesis describes a critical field investigation of aluminum ($T_c \simeq 1.2^{\circ}K$) as a function of temperature and pressure. In the remaining four sections of this chapter, we will discuss the

relationships between critical field measurements and thermodynamic properties of superconductors, and previous measurements in aluminum and other superconductors.

B. Thermodynamic Properties of Superconductors at Constant Pressure

In this section we shall derive some useful thermodynamic relations and apply them to the problem of extracting superconducting state parameters from critical field data. We mentioned in the previous section that the superconducting transition is reversible, and that the methods of reversible thermodynamics are applicable to it. We shall assume, for ease of analysis, that the superconducting specimen is ellipsoidal in shape, and that the magnetic field is parallel to its axis. Hence, the magnetization is uniform in the specimen. We shall also assume that the external field is provided by a solenoid. The final results are independent of these assumptions.[5/] All quantities are expressed in cgs units. Let

P = pressure

H = magnetic field at the sample due to external sources, not including any effects due to the magnetic properties of the sample

T = absolute temperature

V = volume

I = magnetic moment of sample

M = magnetization = I/V

S = entropy.

The amount of work done by the sample to change its magnetic moment by dI is just

$$dW = -HdI \ . \tag{3}$$

The law of conservation of energy for a reversible process may be written

$$TdS = dU + PdV - HdI \ . \tag{4}$$

Now define a magnetic Gibbs potential G, hereafter called the free energy, given by

$$G = U - TS + PV - HI \ . \tag{5}$$

Differentiating, and substituting from (4), we get

$$dG = VdP - SdT - IdH \ . \tag{6}$$

Hence at constant temperature and pressure for an ellipsoidal specimen,

$$G(T,P,H) = G(T,P,0) - V\int_0^H MdH \ . \tag{7}$$

From Figure 1 it is evident that for an ellipsoid,

$$G_s(T,P,H_c) = G_s(T,P,0) + VH_c^2/8\pi, \tag{8}$$

where the subscript s(n) denotes the superconducting (normal) state. At H_c we must have

$$G_n(T,P,H_c) = G_s(T,P,H_c), \tag{9}$$

for the two phases to be in equilibrium. But to a very good approximation

$$G_n(T,P,H_c) = G_n(T,P,0), \tag{10}$$

since the normal state magnetic susceptibility is of the order of 10^{-6}. Hence we find

$$G_n - G_s = VH_c^2/8\pi = \Delta G \ . \tag{11}$$

Using the relation

$$S = -\left(\frac{\partial G}{\partial T}\right)_{P,H} \tag{12}$$

we find

$$\Delta S = -\frac{VH_c}{4\pi}\left(\frac{\partial H_c}{\partial T}\right)_P \ . \tag{13}$$

Since $H_c = 0$ at $T = T_c$, $\Delta S = 0$ at T_c. By the third law of thermodynamics, ΔS must be zero at $T = 0$. Hence there is a latent heat ($T\Delta S$) associated with the superconducting transition which vanishes at $T = 0$ and $T = T_c$. It is interesting to note that the requirement $\Delta S(T=0) = 0$ implies that $\frac{dH_c}{dT} = 0$ at $T = 0$.

The specific heat is given by

$$C = T\left(\frac{\partial S}{\partial T}\right)_P \ . \tag{14}$$

Hence, from (13),

$$\Delta C = -\frac{VT}{4\pi} H_c \left(\frac{\partial^2 H_c}{\partial T^2}\right)_P - \frac{VT}{4\pi}\left(\frac{\partial H_c}{\partial T}\right)_P^2 . \qquad (15)$$

Equation (15) may be evaluated at $T = T_c$ to give

$$\Delta C(T_c) = -\frac{VT_c}{4\pi}\left(\frac{\partial H_c(T_c)}{\partial T}\right)_P^2, \qquad (16)$$

a result known as Rutgers' relation. Since $\Delta S(T_c) = 0$, the transition at T_c is second order; the specific heat discontinuity being given by (16).

The above results are based solely on thermodynamic reasoning. We have seen that differences in thermodynamic quantities between the normal and superconducting states may be calculated from measurements of the critical field curve, using equations (11) through (16). To extract thermodynamic quantities (such as the specific heat) for either the normal or the superconducting state, further assumptions not obtainable through thermodynamic reasoning must be made about the nature of these quantities. The assumptions must be based upon theoretical and experimental evidence concerning the properties of metals at low temperatures. The following assumptions are commonly used in the analysis of calorimetric data as well as critical field data and are generally accepted as giving an adequate description of most experimental evidence.

(i) The specific heat in the normal and superconducting states may be resolved into independent electronic and lattice terms (i.e. $C_n = C_{en} + C_{gn}$, $C_s = C_{es} + C_{gs}$).

(ii) The lattice specific heat remains unchanged in the superconducting transition (i.e. $C_{gs} = C_{gn}$).

(iii) The superconducting electronic specific heat becomes immeasurably small compared to the normal electronic specific heat at low temperatures (i.e. $C_{es} \ll C_{en}$ for $T \ll T_c$).

(iv) The normal electronic specific heat is given by the free electron model (i.e. $C_{en} = \gamma T$, where $\gamma \equiv$ Sommerfeld constant).

Hence, using assumptions (i), (ii), and (iv),

$$\Delta S = S_{en} - S_{es} = \gamma T - S_{es} \tag{17}$$

$$\Delta C = C_{en} - C_{es} = \gamma T - C_{es} \ . \tag{18}$$

And at the lowest temperatures, by assumption (iii),

$$\lim_{T\to 0} \Delta S = S_{en} = \gamma T = C_{en} = \lim_{T\to 0} \Delta C \ . \tag{19}$$

From equation (11),

$$\Delta G = \frac{V H_c^{\,2}}{8\pi} = -\int_0^T \Delta S \, dT + \Delta G(T=0) \quad \cdots\cdots\cdots \tag{20}$$

$$= \Delta G(T=0) - \frac{1}{2}\gamma T^2 + \int_0^T S_{es} dT \quad \cdots\cdots\cdots \tag{21}$$

$$\therefore \quad H_c^2 = H_o^2 - \frac{4\pi\gamma T_c^2}{V}\left[t^2 - 2g(t)\right] \quad \cdots\cdots\cdots \quad (22)$$

$$\left.\begin{aligned} &\text{where} \quad t = T/T_c \\ &\text{and} \quad g(t) = (1/\gamma T_c)\int_0^t S_{es}\,dt \;,\; g(o)=0 \end{aligned}\right\} \quad \cdots\cdots\cdots \quad (23)$$

Using assumption (iii), we introduce the restriction that g(t) goes to zero much faster than t^2 as t goes to zero. In the low temperature limit,

$$H_c^2 = H_o^2 - \frac{4\pi\gamma}{V} T^2 \;. \quad (24)$$

BCS predicts, and it has been found experimentally,[19] that assumption (iii), and thus equation (24) are valid for $t \lesssim .25$. Naturally this cutoff temperature is dependent upon the material being studied. For superconductors with large energy gaps S_{es} is negligible to higher t values than for superconductors with low energy gaps (in units of kT_c).

Provided enough experimental data exist in the region where assumption (iii) is valid, equation (24) can be used to find H_o and γ by fitting the low temperature data to a straight line in H_c^2 and T^2.[19,20] Once H_o and γ are determined, S_{es} and C_{es} may be determined from the data by using equations (13), (15), (17), and (18). If insufficient low temperature data are available, then one must have knowledge of the behavior of g(t) in order to obtain γ and H_o. This, of course, is equivalent to knowing the form for S_{es}, but it turns out that neither γ nor H_o are very sensitive to the details of

g(t) in the region where g(t) is small but not negligible.[21] Thus the final form of S_{es} calculated from the data over the entire temperature range is not too sensitive to its assumed behavior in the region where it is small.

BCS theory predicts values for reduced thermodynamic quantities in terms of the reduced temperature t. The BCS equation for the free energy difference at $0^{o}K$ in terms of the energy gap is

$$\frac{\Delta G}{V} = \frac{1}{2} N(0) \left(\Delta(0)\right)^2 \tag{25}$$

where $N(0)$ = density of states of one spin at the Fermi level per unit volume

$2\Delta(0)$ = energy gap at $0^{o}K$.

Using

$$\gamma = \frac{2}{3} \pi^2 k^2 N(0) V \tag{26}$$

and equation (11), this yields

$$\Delta(0) = H_o \left(\frac{\pi k^2 V}{6\gamma}\right)^{1/2} . \tag{27}$$

Muhlschlegel[22] has shown that the thermodynamic functions which result from the BCS theory may be expressed in terms of

$$a(x) = -\frac{2}{\pi} \int_{-\infty}^{\infty} \log \left(1 + e^{-\pi(x+u^2)^{1/2}}\right) du + x\left(\log \gamma_e \sqrt{x} - \frac{1}{2}\right) + \frac{1}{3} \tag{28}$$

where

$$\left.\begin{aligned} x &= \left(\frac{\Delta(0)}{\pi k T_c}\right)^2 \left(\frac{\Delta(T)}{\Delta(0)} \frac{T_c}{T}\right)^2 \\ \text{and} \quad \Delta(0) &= \frac{\pi}{\gamma_e} k T_c = 1.764\ k T_c \end{aligned}\right\} \tag{29}$$

The BCS equations for the superconducting electronic entropy reduced by γT_c and for the free energy difference reduced by γT_c^2 are

$$S_{es}/\gamma T_c = t\left[1 + 3\left(x\frac{da}{dx} - a\right) - \frac{3x}{2}\right] \tag{30}$$

$$\left(\frac{VH_c^2}{8\pi}\right)\Big/\gamma T_c^2 = \frac{3t^2}{2}\left[x\frac{da}{dx} - a\right] \quad . \tag{31}$$

The reduced energy gap, $\Delta(T)/\Delta(0)$, can be obtained from

$$-\log t = da/dx \quad . \tag{32}$$

The results of Muhlschlegel's calculations of the entropy and critical field are shown in Figures 8 and 9.

C. Previous Measurements of Thermodynamic Properties of Superconductors

For some elements, in particular those with critical temperatures well above $1^{o}K$, excellent critical field and calorimetric data exist. A summary of data for some superconductors is given in Table 1. For these materials it is clear from the table that there is agreement within experimental uncertainty for almost all quantities. That is, the critical field data and calorimetric data are thermodynamically consistent. A particularly detailed analysis of thermodyanmic consistency has been made in the case of tin and indium, and is discussed elsewhere.[19,21]

Table 1

THERMODYNAMIC PROPERTIES OF VARIOUS SUPERCONDUCTORS

Element	Magnetic					Calorimetric*			
	H_o (gauss)	T_c (^oK)	γ $\left(\frac{mj}{mole\ ^oK^2}\right)$	$\left(\frac{\partial H_c(T_c)}{\partial T}\right)_P$ (gauss/^oK)	$\Delta C(T_c)$ $\left(\frac{mj}{mole\ ^oK}\right)$	H_o (gauss)	T_c (^oK)	γ $\left(\frac{mj}{mole\ ^oK^2}\right)$	$\Delta C(T_c)$ $\left(\frac{mj}{mole\ ^oK}\right)$
Pb	802.6±.4[a]	7.193±.005[m]	3.06±.04[a]	-238.4[a]	58.1±.07[a]	806[b]	7.23[b]	2.95-3.3[b,f]	57.7±0.6[c]
Hg	410.88[d]	4.154[d]	1.809[d]	-203.3[d]	18.84[d]	380±60[e]	4.16[e]	1.79[e]-1.86[f]	18.3±0.4[n]
Ta	824[g]	4.479[g]	6.0±.2[g]	-327[h]	41.6[h]	780±4[i]	4.39[i]	5.69[i]	41.5[i]
Sn	305.50[d]	3.722[d]	1.78[d]	-151.7[d]	10.56[h]-10.95[d]	303.4 -306[k]	3.701 -3.722[k]	1.74-1.80[k]	10.6[h]
In	282.66[d]	3.407[d]	1.66[d]	-155.6[d]	9.62[h]-10.09[d]	284-285[k]	3.403[k]	1.59-1.69[k]	9.75

a) Decker, Mapother, and Shaw[24]

b) Daunt and Mendelssohn[25]; Horowitz et al.[37]; Dolecek[38]; van der Hoeven and Keesom[93]

c) Shiffman, Cochran, and Garber[26]

d) Finnemore and Mapother[19]

e) van der Hoeven and Keesom[27]

f) Phillips, Lambert, and Gardner[28]

g) Hinrichs and Swenson[29]

h) Shaw, Mapother, and Hopkins[30]

i) White, Chou, and Johnston[31]

k) Bryant and Keesom[32]; O'Neal and Phillips[33]; Wilkes[34]; Corak and Satterthwaite[35]

l) Clement and Quinnel[36]

m) Franck and Martin[91]

n) Cochran, Shiffman, and Neighbor[92]

*H_o is derived from calorimetric data using $\frac{VH_o^2}{8\pi} = \int_o^{T_c} \Delta S\, dT$

In the case of superconductors with low critical temperatures such as zinc[23] and aluminum the situation is different. The case of aluminum is particularly frustrating because its critical temperature is in the range where He^4 vapor pressure measurements are still feasible, although difficult. A summary of previous data is given in Table 4, Chapter III, together with results from this investigation. The following remarks about the previous data are in order now, however. Of particular interest is a lack of agreement between calorimetric measurements of the specific heat discontinuity at T_c and values calculated from $\left(\frac{\partial H_c(T_c)}{\partial T}\right)_P$. In the case of Hopkins' data[39] and that of Rorer, et al.,[40] the critical field curve near T_c, the specific heat, and the latent heat were measured on the same sample during the same run. Both experiments yielded thermodynamically consistent results. However, both these measurements were made on bulky samples with large demagnetizing factors. All the other magnetic measurements were made on long thin specimens with small demagnetizing factors, and they give consistently higher values for $\Delta C(T_c)$ than the calorimetric measurements. Hopkins and Mapother[39] have mentioned that superheating effects might be more serious for long thin samples, thus causing erroneous results for $H_c(T)$. The following qualifying remarks should be made about the data of Cochran and Mapother.[41] The value listed in Table 4 for $\left(\frac{\partial H_c(T_c)}{\partial T}\right)_P$ is that given in the table of results in their paper. Reanalysis using only points with H_c less than ten gauss gives a lower value, as Cochran and Mapother pointed out in their paper, but there is considerable uncertainty due to a large amount of scatter in the low-field data. The

data of Caplan and Chanin[42] give a lower value, but in their data also there is a lot of scatter close to T_c. There is also some question about the validity of their method of measuring equilibrium values of H_c.

Another feature of the aluminum data is the lack of agreement in measurements of T_c. Values range all the way from $1.16^{\circ}K$ to $1.2^{\circ}K$, although the more recent measurements seem to cluster between $1.175^{\circ}K$ and $1.185^{\circ}K$. Some of the other T_c values, such as that of Cochran and Mapother, may be due to errors in temperature measurement.[43]

The only low temperature magnetic data for aluminum sufficiently precise to show the deviation of the critical field curve from parabolicity is that of Caplan and Chanin,[42] but below $t^2 = 0.1$ there exist large systematic uncertainties in their temperature measurement which make extrapolation to $t^2 = 0$ difficult.

Evidently there still exists a need for precise critical field measurements of aluminum over a wide temperature range.

D. Effects of Pressure on the Thermodynamic Properties of Superconductors

Differences in mechanical properties between the normal and superconducting states can be calculated in much the same fashion as the differences in thermal properties were calculated in Section B. from equation (6),

$$\left(\frac{\partial G}{\partial P}\right)_{T,H} = V \ .$$

Differentiating equation (11), we get

$$\Delta V = V_n(T,P) - V_s(T,P,0) = V_s(H_c)\,\frac{H_c}{4\pi}\left(\frac{\partial H_c}{\partial P}\right)_T + \frac{H_c^2}{8\pi}\left(\frac{\partial V_s(H_c)}{\partial P}\right)_{T,H} \tag{34}$$

The second term on the right hand side of (34) is due to magnetostriction in the superconducting state and is small compared to the first term.[44] Defining

$$\beta = \frac{1}{V}\left(\frac{\partial V}{\partial T}\right)_{P,H} = \text{thermal expansion coefficient} \tag{35}$$

$$K = -\frac{1}{V}\left(\frac{\partial V}{\partial P}\right)_{T,H} = \text{isothermal compressibility,} \tag{36}$$

we find upon differentiating (34), ignoring second-order effects

$$\beta_n - \beta_s = \frac{1}{4\pi}\left(\frac{\partial H_c}{\partial T}\right)_P\left(\frac{\partial H_c}{\partial P}\right)_T + \frac{H_c}{4\pi}\,\frac{\partial^2 H_c}{\partial P \partial T} \tag{37}$$

$$K_n - K_s = -\frac{1}{4\pi}\left(\frac{\partial H_c}{\partial P}\right)_T^2 - \frac{H_c}{4\pi}\left(\frac{\partial^2 H_c}{\partial P^2}\right)_T \tag{38}$$

Equations (34), (37), and (38) can be thought of as special cases of more general equations relating changes in length, elastic constants, and linear expansion coefficients to derivatives of H_c with respect to components of the stress tensor. Seraphim and Marcus[45] have thoroughly analyzed the problem for various crystal symmetries, and we shall not comment further on the more general relations.

Using

$$\left(\frac{\partial^2 G}{\partial P \partial T}\right)_H = \left(\frac{\partial^2 G}{\partial T \partial P}\right)_H \tag{39}$$

it is easily shown that

$$\left(\frac{\partial S}{\partial P}\right)_{T,H} = -\left(\frac{\partial V}{\partial T}\right)_{P,H} . \tag{40}$$

Hence

$$\beta = -\frac{1}{V}\left(\frac{\partial S}{\partial P}\right)_{T,H} . \tag{41}$$

Evidently the assumptions made in Section B regarding the resolution of the specific heat into electronic and lattice terms, etc., may be applied with equal validity to the thermal expansion coefficient, β. Thus, for example,

$$\beta_{en} = -\frac{T}{V}\frac{d\gamma}{dP} = \frac{K_n \gamma T}{V}\frac{d\ln\gamma}{d\ln V} = \frac{K_n C_{en}}{V}\frac{d\ln\gamma}{d\ln V} . \tag{42}$$

Similarly, if $C_{gn} \propto \left(\frac{T}{\theta_D}\right)^3$,

$$\beta_{gn} = -\frac{K_n C_{gn}}{V}\frac{d\ln\theta_D}{d\ln V} . \tag{43}$$

Hence several different types of measurements can be correlated thermodynamically:

(i) The volume or length change at the transition can be measured and compared with direct measurements of the change in H_c with pressure or stress.

(ii) Changes in the thermal expansion coefficient, compressibility, and related quantities such as elastic constants and sound velocities can also be compared with, or deduced from, measurements of the change of H_c with pressure or stress.

(iii) Measurements of the low-temperature behavior of $\left(\frac{\partial H_c}{\partial P}\right)_T$ can give information about $\frac{d\gamma}{dP}$ and can be correlated with the normal electronic thermal expansion coefficient. Once β_{en} is known, β_{es} can be found through (31) from measurement of $H_c(T)$ and $\left(\frac{\partial H_c}{\partial P}\right)_T$ over a wide temperature range.

Swenson[20] has considered the problem of extracting $\frac{d\gamma}{dP}$ from the low temperature data on the pressure dependence of H_c in the following manner. Differentiating equation (24),

$$\left(\frac{\partial H_c^2}{\partial P}\right)_T = \left(\frac{\partial H_o^2}{\partial P}\right)_T - 4\pi T^2 \left(\frac{\partial}{\partial P}\ (\gamma/V)_T\right). \tag{44}$$

Note that

$$\left(\frac{\partial}{\partial P}\ (\gamma/V)\right)_T = \frac{1}{V}\left[\frac{\partial\gamma}{\partial P} + \gamma K_n\right] = \frac{-\gamma K_n}{V}\left[\frac{\partial \log\gamma}{\partial \log V} - 1\right]. \tag{45}$$

Hence at low enough temperatures one may calculate $\frac{d\gamma}{dP}$ from the slope of an experimental plot of $2H_c \frac{\partial H_c}{\partial P}_T$ versus T^2. The deviation of such a plot from a straight line may be estimated by differentiating (21).

$$\left(\frac{\partial H_c^2}{\partial P}\right)_T - \left(\frac{\partial H_o^2}{\partial P}\right)_T + 4\pi T^2 \left(\frac{\partial}{\partial P}\ (\gamma/V)\right)_T = 8\pi \int_0^T \left(\frac{\partial}{\partial P}\left(\frac{S_{es}}{V}\right)\right)_T dT \cong -8\pi \int_0^T \beta_{es}\, dT. \tag{46}$$

Swenson[20] has shown that for tin β_{es} is roughly equal to β_{en} at $t = 0.3$. Hence one would expect the integral on the right hand side of (46) to be appreciable at that temperature.

The functional dependence of $\left(\frac{\partial H_c}{\partial P}\right)_T$ on temperature may be examined in the light of BCS theory. First let us define a similarity principle for critical field curves. Let

$$H_c = H_o f(t). \tag{47}$$

Then, if the pressure dependence is such that

$$H_c(P) = H_o(P) f(t) \tag{48}$$

and f(t) is independent of pressure, then the family of critical field curves at different pressures is said to obey the principle of simple similarity. That is, in terms of the reduced variables H_c/H_o and T/T_c the critical field curve is independent of pressure.

Let us mention in passing a second similarity condition which was useful in interpreting the isotope effect, but is only of historical interest here. If, in addition to simple similarity we have

$$\frac{H_o(P)}{T_c(P)} = \frac{H_c(0)}{T_c(0)} , \tag{49}$$

then the family of critical field curves is said to obey the principle of double similarity.[45]

BCS theory predicts that the deviation from simple similarity will be immeasurably small. From equation (22),

$$\frac{H_c}{H_o} = \left[1 - \frac{4\pi\gamma T_c^2}{VH_o^2}\{t^2 - 2g(t)\}\right]^{1/2} . \qquad (50)$$

It was stated in Section B that BCS makes definite numerical predictions for $\frac{4\pi\gamma T_c^2}{VH_o^2}$ (from equations (27) and (29)) and g(t) (from equation (30)). Actually, these quantities are weakly dependent upon the ratio T_c/θ_D, where θ_D is the Debye temperature. Seraphim and Marcus[45] calculate from BCS that the maximum shift of f(t) is

$$\left.\frac{\partial f}{\partial P}\right)_t \simeq 10^{-4} \frac{\partial \ln(T_c/\theta_D)}{\partial P} \approx 10^{-9} - 10^{-10} \text{ per atmosphere} \qquad (51)$$

for typical superconductors. If we define a deviation function

$$D(t) = H_c/H_o - (1 - T^2/T_c^2) = f(t) - 1+t^2 . \qquad (52)$$

Then,

$$\left.\frac{\partial D_{max}}{\partial P}\right)_t = \left.\frac{\partial f}{\partial P}\right)_t \simeq 10^{-10} \text{ per atmosphere} . \qquad (53)$$

Hence for a pressure of 1000 atmospheres,

$$\Delta D_{max} \sim 10^{-7} , \qquad (54)$$

which for aluminum corresponds to about 10^{-5} gauss, and is thus immeasurably small. Experiments on various superconductors, however, show that the deviation function at zero pressure varies more from material to material than the variation in T_c/θ_D would yield through the BCS theory. Decker, Mapother, and Shaw[24] have found empirically that the maximum value of D(t) varies with $\frac{T_c}{\theta_D}$ such that

$$\Delta D_{max} \cong \Delta(T_c/\theta_D) \ . \tag{55}$$

Thus

$$\left.\frac{\partial D_{max}}{\partial P}\right)_t \cong \frac{T_c}{\theta_D} \frac{\partial \ln(T_c/\theta_D)}{\partial P} \approx 10^{-7} - 10^{-8} \text{ per atmos.} \tag{56}$$

This is still an extremely small effect. Very accurate measurements at pressures on the order of 10,000 atmospheres or greater would be required to measure this shift in aluminum. The situation would not be quite so bad in tin. Seraphim and Marcus[45] give for tin,

$$\frac{\partial \ln(T_c/\theta_D)}{\partial P} \approx 10^{-5} \text{ per atmosphere.} \tag{57}$$

Using[19]

$$T_c/\theta_D = .019 \tag{58}$$

we get

$$\left.\frac{\partial D_{max}}{\partial P}\right)_t \cong 2\times10^{-7} \text{ per atmosphere} \ . \tag{59}$$

Hence if $P \sim 10{,}000$ atmospheres,

$$\Delta D_{max} \simeq .002 \tag{60}$$

In tin this corresponds to about 0.6 gauss, which with high precision techniques could possibly be observed. To our knowledge, all pressure effect experiments on superconductors published to date give results which are consistent with simple similarity.

Consider the consequences of simple similarity. From equation (50), we see that if simple similarity holds,

$$\frac{\gamma^* T_c^2}{H_o^2} = \text{constant, where } \gamma^* = \frac{\gamma}{V} . \tag{61}$$

Note that double similarity would not be expected to hold, since the density of states at the Fermi level, and hence γ, are functions of volume and pressure. Double similarity is obeyed in the isotope effect, however, since N(o) is not a function of isotopic mass. Differentiating (61), we find

$$\frac{d\ln\gamma^*}{dP} = \frac{2\ d\ln H_o}{dP} - \frac{2\ d\ln T_c}{dP} . \tag{62}$$

Using

$$\frac{dT_c}{dP} = -\left(\frac{\partial H_c(T_c)}{\partial P}\right)_T \Big/ \left(\frac{\partial H_c(T_c)}{\partial T}\right)_P \tag{63}$$

we then get

$$\frac{1}{\gamma^*}\frac{d\gamma^*}{dP} = \frac{2}{H_o}\left(\frac{\partial H_c(T_c)}{\partial P}\right)_T \left[\frac{dH_o/dP}{(\partial H_c(T_c)/\partial P)_T} + \frac{H_o}{T_c}\ \frac{1}{(\partial H_c(T_c)/\partial T)_P}\right] . \tag{64}$$

Hence if simple similarity holds we do not need equation (44) and an experimental plot of $2H_c\left(\frac{\partial H_c}{\partial P}\right)_T$ vs. T^2 at very low temperatures to find $\frac{d\gamma^*}{dP}$. However, we still must extrapolate to t = 0 to obtain the pressure dependence of H_o. This can be done by using the experimental plot described above and equation (44) or by simply extrapolating a

plot of $\left(\frac{\partial H_c}{\partial P}\right)_T$ versus t^2 to zero. The shape of such a plot under the restriction of simple similarity can be found by differentiating equation (47). Substituting (52) and differentiating,

$$\left(\frac{\partial H_c}{\partial P}\right)_T = \frac{\partial H_o}{\partial P}\left[1 + \left(2\,\frac{d\ln T_c/dP}{d\ln H_o/dP} - 1\right) t^2 + D(t) - 2t^2\,\frac{\partial D}{\partial t^2}\,\frac{d\ln T_c/dP}{d\ln H_o/dP}\right] \tag{65}$$

where we have used the fact that

$$\left(\frac{\partial t}{\partial P}\right)_T = -t\,\frac{d\ln T_c}{dP} \quad . \tag{66}$$

The last two terms on the right hand side are typically a few percent of the first two terms. Thus $\left(\frac{\partial H_c}{\partial P}\right)_T$ is very nearly a straight line in t^2 over the entire range of t, although the slope of a best straight line fit to an experimental plot of $\left(\frac{\partial H_c}{\partial P}\right)_T$ vs. t^2 may be affected by the last term in (65), and thus will not be given by the coefficient of the second term in (65). The percentage error involved in finding dH_o/dP and $\left(\frac{\partial H_c(T_c)}{\partial P}\right)_T$ by fitting such a plot to a straight line in t^2 is small, on the order of 5%.

The variation of T_c with pressure can be studied by means of the BCS relation

$$T_c \simeq 1.14\,\theta_D\, e^{-\frac{1}{N(o)A}} \tag{67}$$

where A is the BCS electron-electron coupling constant. Thus

$$\frac{d\ln T_c}{d\ln V} = \frac{d\ln\theta_D}{d\ln V} + \frac{1}{N(0)A}\left[\frac{d\ln N(0)}{d\ln V} + \frac{d\ln A}{d\ln V}\right] . \tag{68}$$

Solving for $\frac{d\ln A}{d\ln V}$, remembering that $\frac{\gamma}{V} \propto N(o)$,

$$\frac{d\ln A}{d\ln V} = N(o)A\left[\frac{d\ln T_c}{d\ln V} - \frac{d\ln\theta_D}{d\ln V}\right] + 1 - \frac{d\ln\gamma}{d\ln V} . \qquad (69)$$

Hence the volume dependence of A can be calculated from experimental measurements of the volume dependence of T_c, θ_D, and γ. Unfortunately, experimental uncertainties in such measurements lead to large uncertainties in calculated values of $\frac{d\ln A}{d\ln V}$, thus making comparison with theoretical estimates difficult.[46]

E. Previous Pressure Effect Measurements on Aluminum

Pressure effect measurements on superconductors have been so thoroughly reviewed elsewhere[47,48,49] that we shall confine our remarks to previous results in aluminum. These results are given in Table 6, Chapter III. The values of $\frac{d\ln\gamma}{d\ln V}$ listed for Olsen[50] and for Gross and Olsen[51] were calculated from measurements of $\left(\frac{\partial H_c}{\partial P}\right)_T$ by fitting their data to $\left(\frac{\partial H_c}{\partial P}\right)_T = a + bt^2$ and using equation (64) based upon simple similarity. The discrepancy in $\frac{d\ln\gamma}{d\ln V}$ of over an order of magnitude between Olsen's result and that of Gross and Olsen is surprising. The two experiments were very similar. In both experiments two aluminum samples were used; one under pressure in an ice bomb and the other at zero pressure. Differences in the critical field of the two samples were directly measured as a function of temperature down to $0.3^{o}K$ with a fixed pressure in the ice bomb. In the Gross and Olsen experiment two different sets of aluminum samples were measured.

The only difference between the two experiments was in the pressure calibration. In the Olsen experiment the difference in the critical field of two cadmium specimens, one in the ice bomb and one at zero pressure, was used to measure the pressure. The pressure was calculated from earlier measurements on cadmium by Alekseevskii and Gaidukov.[52] Gross and Olsen used two indium specimens instead, and mentioned in their paper that due to anisotropy in the pressure effect in cadmium, the pressure calibration at low temperatures in the Olsen experiment was erroneous. It is hard to see, though, how an error in pressure calibration could affect the ratio $\frac{dH_o}{dP} \Big/ \left(\frac{\partial H_c(T_c)}{\partial P}\right)_T$. The pressure in the bomb should not change appreciably with temperature. It appears that the results of Gross and Olsen are in much better agreement with the low temperature thermal expansion measurements of Andres[53] and of White.[54]

II. EXPERIMENTAL APPARATUS AND PROCEDURE

A. Background

A few measurements[29,55,56] of the effect of pressure on critical field curves have been reported in which solid helium was used to transmit hydrostatic pressure to a sample. Solid helium has two principle advantages as a low temperature pressure transmitter. It is a soft, highly compressible solid, and as a result inhomogeneous stresses tend to anneal out. Also, for pressures below 10,000 psi, the melting curve lies below 15°K. Thus the high-pressure bomb can be pressurized while the experiment is at low temperatures, and measurements can be made at more than one pressure during a low temperature run.

Garfinkel and Mapother[56] have described an apparatus using solid helium as a pressure transmitter with which they have measured the effect of pressure on the critical field curve of lead at temperatures down to 1°K. They developed a capacitance technique for measuring the extension of their high pressure bomb under pressure, thus avoiding the use of a specimen of another superconductor in which $\left(\frac{\partial H_c(T)}{\partial P}\right)_T$ is assumed to be known in order to measure the pressure. They measured the critical field curve of their lead sample at fixed pressure without the use of a comparison sample at zero pressure. This necessitates temperature measurements of high precision in order that accurate critical field differences can be obtained from critical field curves measured at different pressures.

We have adapted the Garfinkel and Mapother technique for use with a He^3 refrigerator capable of reaching temperatures as low as $0.3^{\circ}K$, thus making measurements on aluminum possible over a wide range of reduced temperatures, at pressures ranging from zero to about 10,000 psi. In the sections to follow we will discuss the essential points of the technique.

B. Sample Preparation

The aluminum sample was a 1.25 inch length cut from 0.080 inch diameter 99.9999% pure polycrystalline aluminum wire supplied by Comirco Products, Inc. of Spokane, Washington. After cutting, the sample was cleaned and its ends rounded in a 10N solution of NaOH followed by a distilled water rinse.

The sample was then annealed for 20 hours at $633^{\circ}C$ in a CO_2 atmosphere, after which it was cooled to room temperature at a rate of $27^{\circ}C$ per hour. The CO_2 provided a reducing atmosphere which stabilized the oxidation of the sample surface. The sample was then recleaned as before and placed in the cryostat.

C. Low Temperature Apparatus

In this section we will discuss the construction of the high pressure bomb, the He^3 refrigerator, and the resistance and magnetic thermometers, and the method for obtaining thermal contact between various parts of the cryostat. How the apparatus is used will be discussed in later sections.

The apparatus, which is cryogenically quite similar to that described by Finnemore and Mapother,[19] is shown in Figure ?. During the experiment it is immersed in a bath of liquid He^4. Thermal isolation between the He^4 bath and the He^3 refrigerator is maintained by high vacuum between the outer and inner cans. Also, all tubes and leads connecting the inner system to the He^4 bath are made from long lengths of thin-wall cupronickel tubing and poorly conducting manganin wire to keep the heat leak as low as possible. When good thermal contact is desired between the inner and outer cans, He^4 gas is admitted to the outer can.

The He^3 evaporation chamber is made from copper. It is silver-soldered to the top of the inner can and has a 2000 ohm manganin heater wound around it in bifilar fashion. The sample is held in place by nylon spacers in a brass sample holder, which in turn is screwed into the tellurium copper thermal ground. The thermal ground projects through the beryllium copper flange and is screwed into the bottom of the He^3 evaporation chamber with Apiezon N-grease on the threads to improve thermal contact. The thermal ground and beryllium copper flange were silver soldered together before final machining. The bomb itself is the same as that described by Garfinkel and Mapother. It was machined from beryllium copper to an OD of 0.456 inches and an ID of 0.375 inches, and heat-treated to an ultimate tensile strength of 200,000 psi. The hardened bomb was calculated to have a bursting pressure of about 30,000 psi. The high pressure seal is made by compressing the Teflon gasket against the

Figure 2. Cross-section of cryostat.

A. outer can

B. He^3 evaporation chamber

C. inner system heater

D. bucking coil

E. beryllium copper plug

F. flange

G. thrust washer

H. Teflon gasket

I. high pressure bomb

J. copper yoke

K. sample coil

L. thermal ground

M. sample

N. inner can

O. high pressure capillaries

P. Speer carbon resistor

Q. capacitor plates

R. epibond insulator

S. salt pill primary coil

T. salt pill secondary coils

U. salt pill

V. nylon spacer

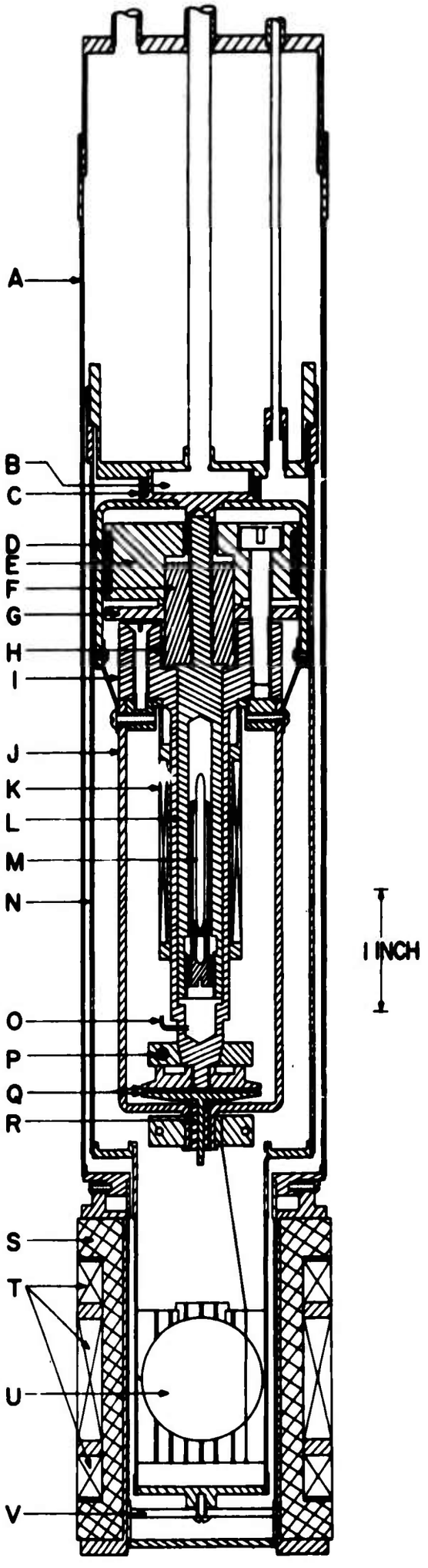
A
B
C
D
E
F
G
H
I
J
K
L
M
N
O
P
Q
R
S
T
U
V
1 INCH

beryllium copper flange and the wall of the bomb. The gasket is compressed by a beryllium copper thrust washer, clamped in position by a beryllium copper plug which is bolted to the bomb with five #8-32 beryllium copper bolts. All beryllium copper pieces were heat-treated in the same manner as the bomb. The seal design makes use of the "unsupported areas" principle of Bridgman.[57] It is characteristic of this type of seal that the internal pressure in the gasket is always greater than the internal pressure in the bomb by a fixed ratio, thus creating a positive seal which should improve as the pressure is increased. Due to the large thermal contraction in the Teflon gasket, it is necessary to preload the gasket before cooling t helium temperatures. The bolts are tightened such that the gasket i aded with about 5000 pounds force at room temperature, which corresponds to about 5000 atmospheres pressure in the gasket. According to Swenson,[58] this should be enough to prevent unloading of the gasket at low temperatures. The seal was found to be satisfactory at pressures up to 10,000 psi at helium temperatures. However, leakage occured above this pressure. The reason for this is not known. However, 10,000 psi was close enough to the maximum working pressure of the high pressure gas handling equipment (see Section E) that it was not deemed necessary to improve the seal for this experiment.

Helium gas is admitted to the bomb through one of the cupronickel tubes soft-soldered into the bomb. The method by which the helium is pressurized and solidified in the bomb will be discussed

in Section E. Thermal contact between the specimen and the tellurium copper thermal ground is made by the solid helium in the bomb. For measurements at zero pressure, He^3 exchange gas is admitted to the bomb at a pressure of a few psi at liquid helium temperature.

Two thermometers are used in this apparatus; a 470 ohm ½ watt Speer carbon resistor and a spherical pill of paramagnetic salt. The carbon resistor is mounted in a copper ring which is clamped to the bottom of the bomb. Apiezon N-grease is used to promote thermal contact between the copper ring and the bomb. The salt pill is made up of a mixture of fine crystals of chrome methylamine alum and Dow Corning silicon oil packed into a nylon form. The silicon oil improves thermal contact between salt crystals and inhibits the loss of the water of hydration by the salt. The mixture is 76% salt by volume. Thermal contact to the salt is made by 32 #20 copper wires which penetrate the salt-oil mixture. These wires emerge from the nylon form and are silver soldered into a copper clamp, which is coated with N-grease and tightly clamped to a copper yoke. The yoke is thermally grounded to the He^3 refrigerator. All electrical leads, which are 0.0031 inch diameter enamel-covered manganin wire, are also thermally grounded to the copper yoke. Also, during a run the inner can is filled with He^3 exchange gas to improve thermal contact between bomb, refrigerator, and thermometers. We find that at all temperatures with the above arrangement the carbon resistor and the magnetic salt respond within a few seconds to pulses of heat put into the He^3 refrigerator by the electrical heater. Hence we conclude that the bomb, refrigerator, and thermometers are in good thermal contact.

D. Critical Field Measurements

We detect magnetic transitions under isothermal conditions using a ballistic induction technique. This technique has been thoroughly described elsewhere,[59] and will only be briefly reviewed here. Two separate solenoids are used to provide a magnetic field at the sample. One solenoid, called the nitrogen solenoid because it is located in the nitrogen bath which surrounds the helium dewar, produces a large constant field (up to 1000 gauss) at the sample. The other solenoid, called the air solenoid because it is situated outside the dewar system, produces a small field (less than 10 gauss) which may be made to add or subtract from the large field. The field produced by these solenoids is uniform to 6 parts in 10,000 over the volume of the sample, and is calibrated to 3 parts in 10,000. Corrections for the inhomogeneity introduced by the magnetic salt and small amounts of superconducting solder in the cryostat were calculated to be negligible. Stray magnetic fields were canceled to $\pm$ .04 gauss with a Helmholtz pair. Two search coils, called the sample coil and the bucking coil (see Figure 2), are used. The sample coil, having 11,900 turns of #44 copper magnet wire wound with an average radius of 0.655", surrounds the sample. The bucking coil has 1958 turns of #44 copper magnet wire wound with an average radius of 1.563", and is located well away from the sample. The area-turns products for these two coils are equal. The two coils are connected in series opposition through a ballistic galvanometer. The galvanometer used in this experiment is a Kipp model A-54 double coil

galvanometer, made by P. J. Kipp and Zonen of Delft, Holland. This galvanometer has magnetic shunts which make it possible to vary the CDRX (external resistance which gives critical damping) of either galvanometer coil over a wide range. With the 50 ohm galvanometer coil it is possible to vary CDRX from 1 ohm to 1500 ohms. With the 450 ohm galvanometer coil, the magnetic shunts allow CDRX to be varied from 4000 to 100,000 ohms. Since the galvanometer is used as a fluxmeter, it is desirable to have the CDRX considerably larger than the combined resistance of the two search coils and their leads, which in this case is about 700 ohms at liquid helium temperatures. We found that the best combination of flux sensitivity and fluxmeter behavior was obtained by using the 450 ohm coil at minimum CDRX. The flux sensitivity under the above conditions, and with a 140 cm path between the galvanometer mirror and the galvanometer scale, is about 0.015 mm/gauss cm^2.

The following procedure is used to measure H_c. At a temperature below T_c the nitrogen solenoid field is set at a value close to H_c, and the magnetic field at the specimen is increased by small, monotonic, stepwise increments through H_c using the air solenoid. The effective permeability of the specimen as it makes a superconducting-to-normal transition is determined from the galvanometer deflections accompanying each step, since each is proportional to the flux which enters the sample during that step. The two search coils are perfectly balanced when the sample is normal, and only a slight imbalance exists when the sample is superconducting. This imbalance leads to deflections

which are much smaller than those which occur in the intermediate state, and are neglected. The effective permeability of the sample at the m^{th} step is then defined as

$$\mu_m = \sum_{i=1}^{m} \delta_i \Big/ \sum_{\text{all steps}} \delta_i \qquad (70)$$

where δ_i is the deflection corresponding to the i^{th} step. H_c is then determined by extrapolating an experimental plot of μ versus the applied field to $\mu = 1$. The details of the magnetic transitions and the resulting critical field values will be discussed in the next chapter.

E. High Pressure Generation and Measurement

In this section we will describe the high pressure apparatus external to the cryostat, the pressure lines into the cryostat, the pressure measuring system, and the experimental procedure. The apparatus and techniques are very similar to those of Garfinkel and Mapother.

Helium gas is compressed by an SC model 10-500-16 air-operated hydraulic pump capable of a maximum pressure of 25,000 psi. The compressed gas then passes through a coil of 1/16" ID x 1/8" OD high pressure tubing suspended in a bath of liquid nitrogen, to freeze out impurities in the gaseous helium. All lines and fittings external to the cryostat are High Pressure Equipment Co. midget series

valves, fittings, and tubing with a maximum working pressure of 15,000 psi. After passing through the cold trap the gas is admitted to the high pressure bomb through a capillary. A second capillary goes from the bomb to a Heise high precision Bourdon gauge at room temperature. The use of separate inlet and return lines allows one to know whether or not the lines are blocked. The capillaries are half-hard .018" OD x .008" ID cupronickel tube with a tensile strength of 60,000 psi. The advantages of cupronickel are that it is easily soft-soldered and is non-magnetic. The two capillaries are wound with a 200 ohm manganin non-inductive heater and enclosed in a vacuum jacket which extends from the top of the outer can to well above the helium level. The heater-wound capillaries emerge from the vacuum jacket and enter the inner can through epoxy seals.

A capacitance technique is used to measure the extension of the bomb under pressure. One capacitor plate is attached to the lower end of the bomb, and the other is fixed with respect to the upper end of the bomb. These plates have an area of about .63 square inches and are adjusted at room temperature and zero pressure to have a separation of about 0.010 inches. The change in length of the bomb is about 0.002 inches per 10,000 psi, which results in a capacitance change of about 2×10^{-4} picofarads per psi. The capacitance is measured by comparison with an external General Radio type 1422-ME high precision variable capacitor using a Robertshaw-Fulton capacitance bridge as a null detector. Capacitance changes of about .002 pf, corresponding to about 10 psi, can be measured in this way.

The effects of variable lead capacitance are avoided through the use of a triaxial cable between the capacitance bridge and the bomb capacitor. A schematic diagram of the capacitance measuring system is shown in Figure 3. The inner shield divides the stray capacitance, which is about 20 pf, into two parts. One part, C_{ab}, is a across the output of the bridge and thus has no effect on the bridge balance conditions. The other part, C_{bc}, is effectively in parallel with C_1 which is 1000 pf. Thus variations in bridge output due to variations in stray capacitance are reduced by a factor of about $\frac{1000\ pf}{C_x + C_3 + C_{stray}}$, where $(C_x + C_3 + C_{stray})$ is about 50 picofarads. The construction of the triaxial cable which extends down the cryostat to the bomb capacitor is shown in Figure 4.

The experimental procedure is as follows. The capillary vacuum jacket and the outer can are evacuated, and both the capillary heater and the inner system heater are turned on. The inner system is warmed up to a temperature greater than the solidification temperature of helium at the pressure desired. Approximate temperature values above $4.2^{o}K$ are obtained from the resistance of the Speer resistor clamped to the bomb, but no accurate temperature measurements were attempted. Helium gas is then admitted slowly to the bomb, and the capacitor is calibrated against the external Bourdon gauge. The calibration and pressurization procedure takes about ½ hour. When the pressure reaches the desired level the capillary heater is turned off and helium exchange gas is admitted to the capillary vacuum jacket to bring it into thermal contact with the helium bath, thus

Figure 3. Schematic diagram of capacitance measuring system.

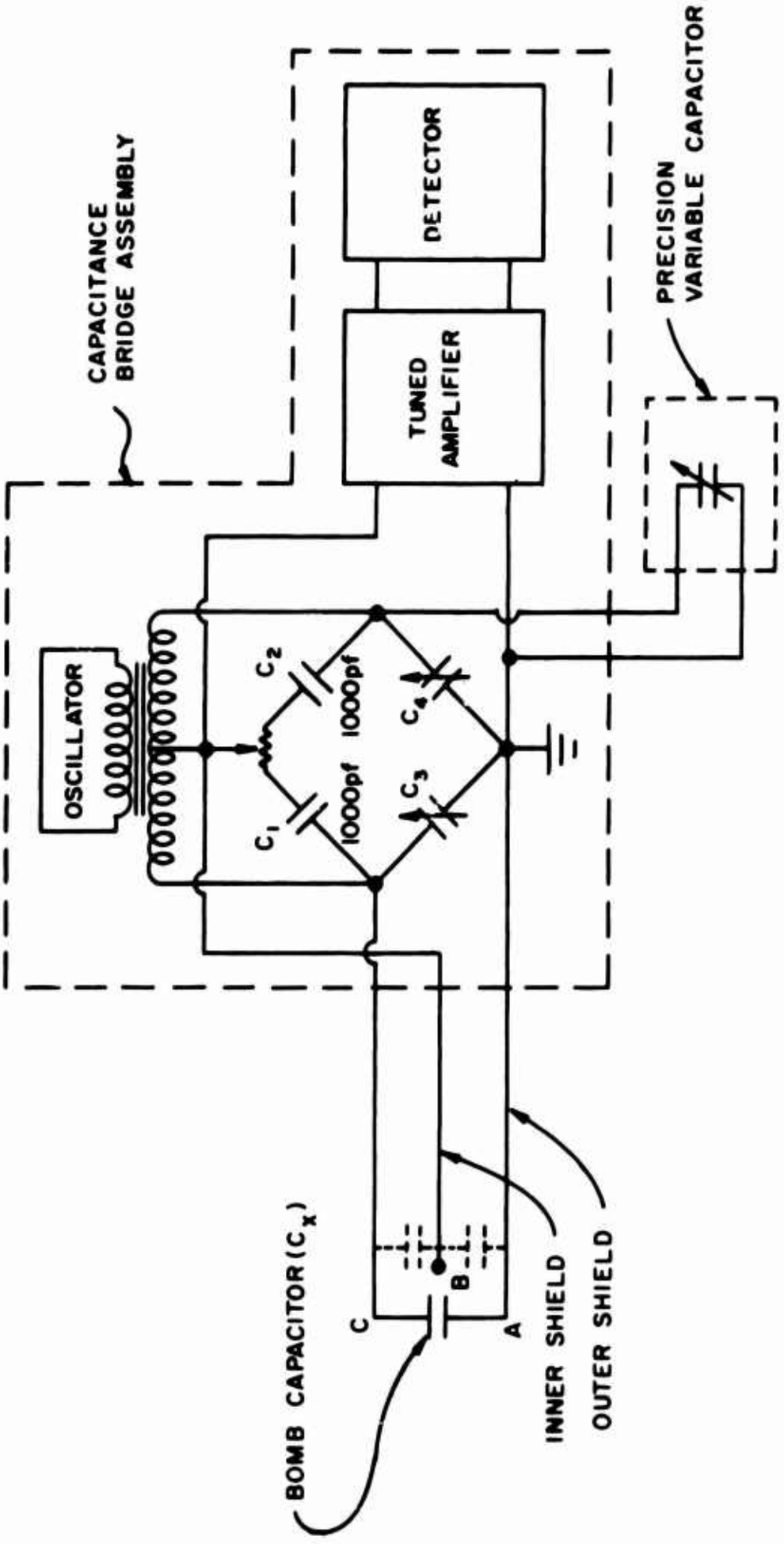
CAPACITANCE
BRIDGE ASSEMBLY
DETECTOR
TUNED
AMPLIFIER
PRECISION
VARIABLE CAPACITOR
OSCILLATOR
C2
1000pf
C4
C1
1000pf
C3
BOMB CAPACITOR (Cx)
C
B
A
INNER SHIELD
OUTER SHIELD

Figure 4. Cross-section of low-temperature portion of triaxial cable.

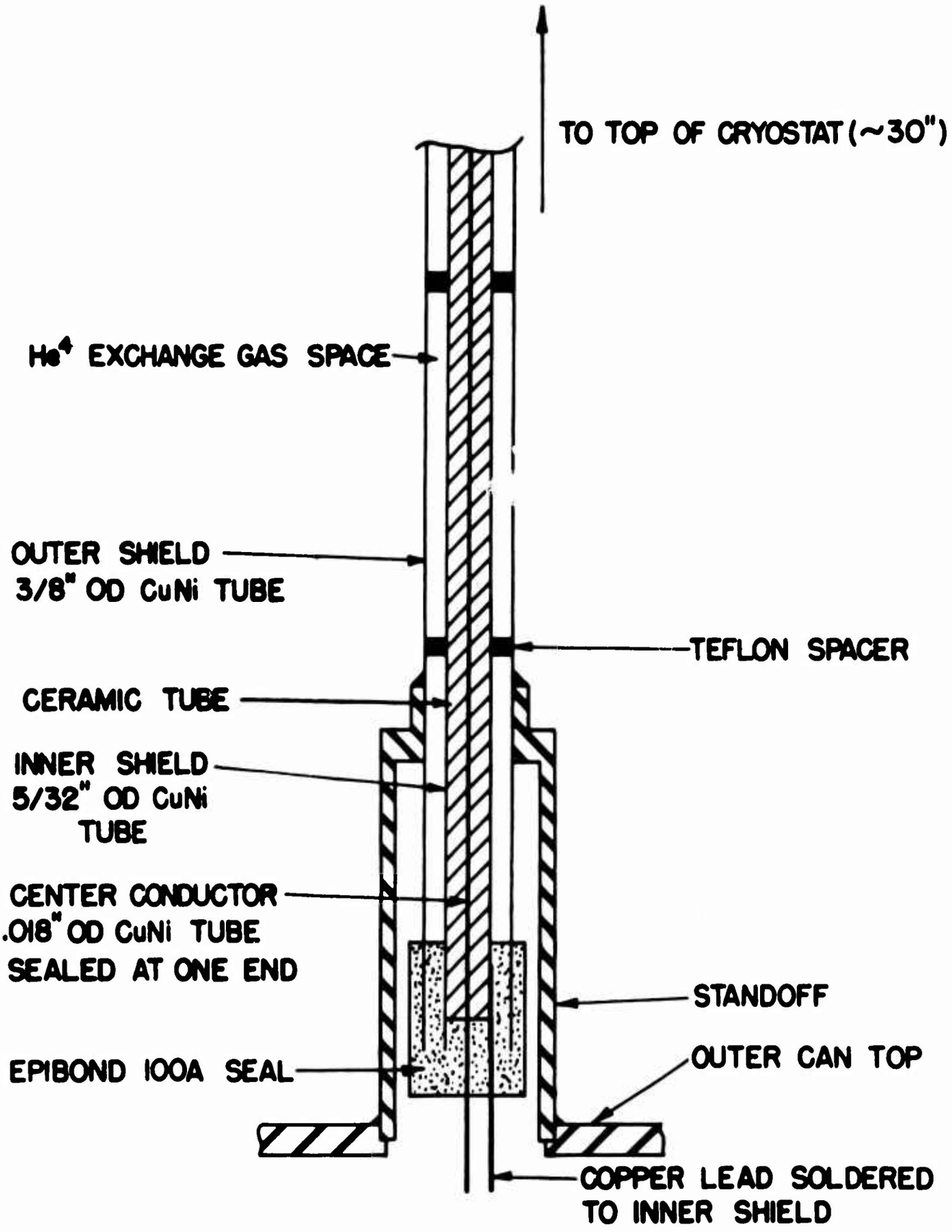
TO TOP OF CRYOSTAT (~30")
He⁴ EXCHANGE GAS SPACE
OUTER SHIELD
3/8" OD CuNi TUBE
TEFLON SPACER
CERAMIC TUBE
INNER SHIELD
5/32" OD CuNi
TUBE
CENTER CONDUCTOR
.018" OD CuNi TUBE
SEALED AT ONE END
STANDOFF
EPIBOND 100A SEAL
OUTER CAN TOP
COPPER LEAD SOLDERED
TO INNER SHIELD

freezing the helium in the capillaries. The inner system heater is then turned off, and the outer can exchange pressure adjusted so that the bomb cools to 4.2°K over a period of several hours, during which time the capacitance is monitored. The result is a curve of capacitance versus Speer resistance such as that shown in Figure 5. Below 4.2°K the thermal expansion of the solid helium is small and the capacitance versus temperature curve is essentially flat. The final pressure of the solid helium on the specimen is taken from the calibration of the bomb capacitor.

The accuracy of the pressure measurement is limited by the stability of the capacitance. We find that the bomb capacitance, after solidification and cooling is complete, is stable to within about $\pm$ .02 pf, or about $\pm$ 100 psi, over a period of several days. The interpolation uncertainty in the bomb calibration is also about $\pm$ 100 psi, and as a result we estimate that our pressure measurements are good to within about $\pm$ 200 psi.

We performed three condensations of the type described here. The final pressures were 3100, 5400, and 7200 psi. The condensations and runs at 3100 and 5400 psi were quite normal; however, the run at 7200 psi showed some unusual features.

(1) There was evidence of some leakage of He^4 from the bomb.

(2) The bomb calibration prior to condensation was done extremely quickly, with all points taken while the pressure was rising rapidly. As a result, it was considered suspect and a new bomb calibration was made after the run, which differed from the

Figure 5. Constant volume condensation of solid helium at 5400 psi.

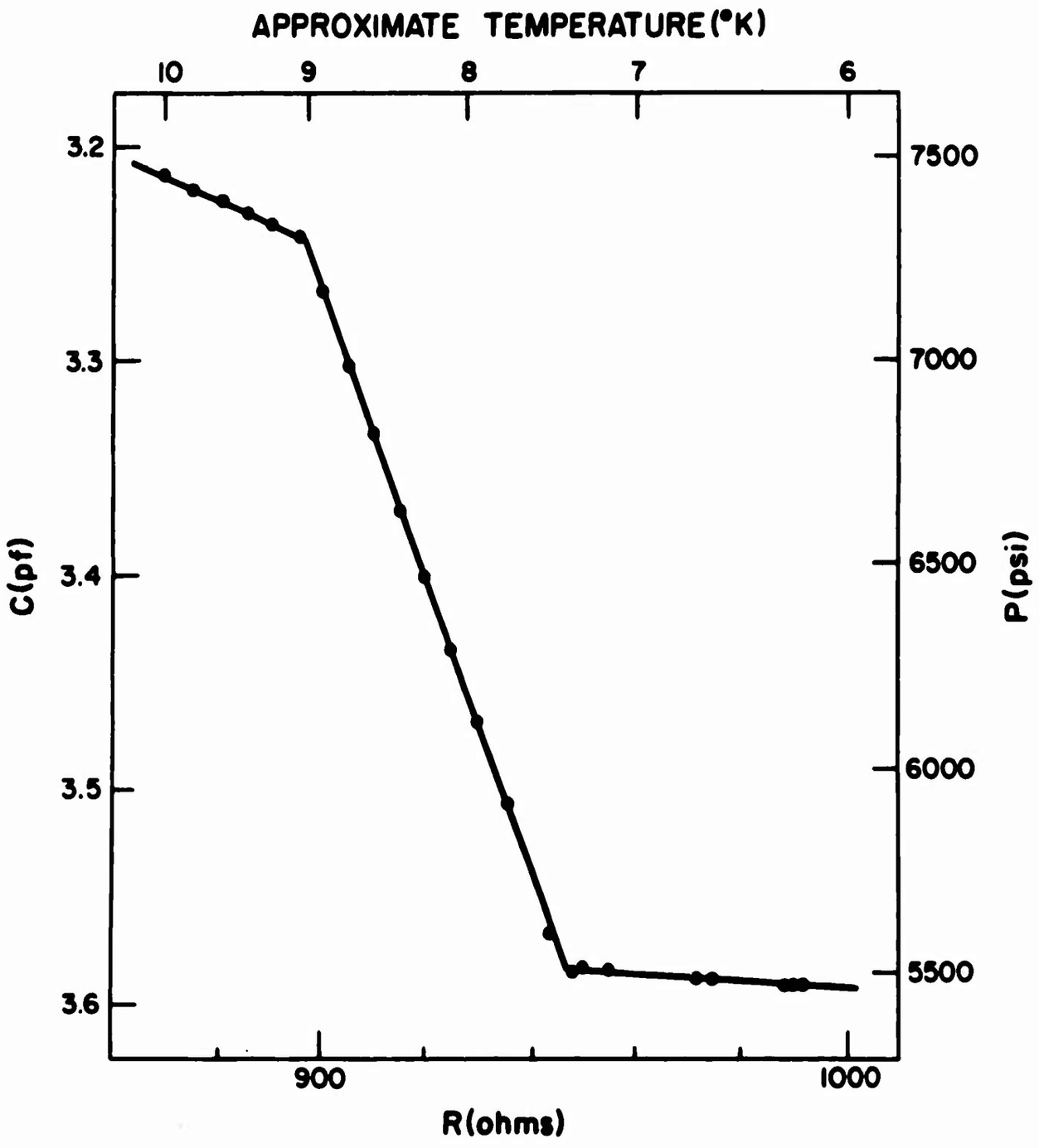
APPROXIMATE TEMPERATURE (°K)
10
9
8
7
6
3.2
3.3
3.4
3.5
3.6
C(pf)
7500
7000
6500
6000
5500
P(psi)
900
1000
R(ohms)

initial one by about 12%. The capacitance of the bomb was monitored throughout the run and remained within the limits mentioned earlier in this section. We thus concluded that any leakage which occurred during the data-taking portion of the run was negligibly small. The second bomb calibration was made much more carefully than the first, and was used to calculate the pressure. The data for this run, which will be discussed in the next chapter, show no anomalies which can be attributed to incorrect pressure calibration, non-constant pressure, or inhomogeneous pressure. Our conclusion is that the data from the 7200 psi run are reliable.

F. Temperature Measurement and Control

The following will be discussed in this section: the procedure and apparatus for making magnetic salt measurements, the calibration of the magnetic salt, and the control and measurement of temperatures below T_c of aluminum.

We determine temperatures below $1.2^{\circ}K$ from the mutual inductance of a set of coils containing the salt pill described in Section C. These coils and the apparatus used to measure their mutual inductance are identical to the system described by Finnemore.[19] The coils, shown in Figure 2, are wound on a bakelite form and attached to the outer can. The secondary coil which surrounds the salt pill is connected in series opposition to the secondaries on either side of it, thus subtracting out most of the temperature-independent mutual inductance. The mutual inductance is given by

$$M = A + B/T^* \tag{71}$$

where T^* is a magnetic temperature differing slightly from the absolute temperature, and B is proportional to the Curie constant of the salt (chrome methylamine alum). The constants A and B vary from run to run, but are typically

$$\left.\begin{aligned} A &= 100 \text{ microhenries} \\ B &= 1000 \text{ microhenry } {}^{\circ}K \end{aligned}\right\} . \tag{72}$$

The mutual inductance is measured by comparing it to a variable mutual inductance with a ballistic Hartshorn bridge to a precision of 1 microhenry. The variable mutual inductance was calibrated with a General Radio type 1632 inductance bridge to a precision of 0.3 microhenry. The calibration procedure has been described previously by Wilkes.[34] To calculate absolute temperatures, magnetic temperatures must be corrected for the difference between applied field and local field, and for the splitting of the energy levels of the Cr^{+++} ions by the crystalline electric field. The local magnetic field correction has been calculated by Onsager[60] and is given by

$$T^*_{ons} = \frac{\left(T^* - \frac{4\pi C}{3V}\right)\left(T^* + \frac{8\pi C}{3V}\right)}{\left(T^* + \frac{4\pi C}{3V}\right)} \tag{73}$$

where C/V is the Curie constant per unit volume of the salt. The Hebb and Purcell[61] relation for the electric field splitting

correction is

$$T = T^*_{ons}\left[\frac{(3 + 4T/\delta) + (3 - 4T/\delta)e^{-\delta/T}}{5(1 + e^{-\delta/T})}\right] \qquad (74)$$

where $\delta = .275^{\circ}K$ for chrome methylamine alum. The resulting $T - T^*$ relation has been verified by experimental determinations of the entropy and specific heat of a powered sample as a function of susceptibility.[62,63] At $1^{\circ}K$, the correction is about $.003^{\circ}K$; at $0.3^{\circ}K$ it is about $.010^{\circ}K$.

The magnetic salt thermometer is calibrated above $1.2^{\circ}K$ against the vapor pressure of He^4 using the 1958 He^4 vapor pressure scale.[64] In this range the He^4 bath temperature is controlled by an automatic pressure regulator and an electrical heater. The automatic pressure regulator serves as the coarse control, and the electric heater as the fine control. The power to the heater comes from a Leeds and Northrop series 60 C.A.T. controller which is driven by the error signal from a DC wheatstone bridge monitoring a carbon resistor in the He^4 bath. Temperatures can be controlled automatically to better than $10^{-4}\ ^{o}K$ using this method. The He^4 vapor pressure is measured with mercury and oil manometers using a Wild cathetometer. A vacuum jacketed probe senses the He^4 vapor pressure a few centimeters over the bath. No points are taken above the λ point of liquid He^4 to avoid uncertainties due to the pressure head of the bath. We typically took twelve salt pill calibration points

between 1.2°K and 2.17°K. The RMS deviation of the calibration points from a best straight line fit in $1/T^*$ was roughly 0.8 microhenry. The constants A and B in equation (71) were determined to about $\pm$ 1 and $\pm$ 1.7, respectively. The effect of the aluminum sample on the mutual inductance was calculated to be about .03 μh, which is negligible.

Below 1.2°K the inner system is isolated from the bath and the temperature is controlled by pumping on liquid He^3 in the He^3 refrigerator and by controlling the power to the 2000 ohm manganin heater wrapped around the He^3 evaporation chamber. The power to the heater is supplied by the L&N C.A.T. controller which is driven by the error signal from an AC wheatstone bridge monitoring the Speer resistor clamped to the bottom of the bomb. The AC bridge operates at 33cps; its output is amplified using the circuit of Blake, Chase, and Maxwell,[65] and detected using the phase sensitive detector designed by Anderson.[66] The power to the thermometer from the bridge is of the order of .01 ergs per second. This compares with a heat leak from all other sources of about 100 ergs per second. The lowest temperatures attainable were about 0.3°K. Over the range from 0.3°K to 1.2°K the temperature could be controlled to 10^{-4} °K or better.

Temperatures were measured with the magnetic salt thermometer. Two low temperature runs were made. On the first run, critical field curves at zero pressure and 3100 psi were measured. During the second run, critical field curves were measured at 5400 psi, 7200 psi, and zero pressure. The temperature measurement procedure was different for the two runs, and the procedure for each run will be described.

Run 1. Magnetic temperatures were measured at roughly half of the critical field points. These were used (after making the $T - T^*$ correction) to calibrate the Speer resistor. The resistor was calibrated by determining the expansion coefficients in

$$\frac{1}{T} = \sum_{n=-1}^{+3} a_n (\ln R)^n \qquad (75)$$

in least squares fashion, using computer programs described by R. E. Harris.[67] The RMS deviation of the data from the fitted curve was $0.0007^{\circ}K$ and $0.0005^{\circ}K$ for the zero pressure and 3100 psi calibrations, respectively. Above $0.8^{\circ}K$ there appeared to be no systematic deviation outside of the data scatter. Hence temperatures between $0.8^{\circ}K$ and $1.2^{\circ}K$ were calculated from the R vs T formula. Below $0.8^{\circ}K$, systematic deviations were larger than the scatter, so temperatures were calculated using the formula plus a small temperature-dependent correction which was always less than $0.0003^{\circ}K$. There also appeared to be a systematic shift of the calibration between the zero pressure and 3100 psi calibration of about $0.002^{\circ}K$ at $0.3^{\circ}K$, but smaller at higher temperatures. We thus calculated temperatures for the zero pressure and 3100 psi critical field points from the zero pressure and 3100 psi calibrations, respectively.

Run 2. On the second run magnetic temperatures were measured at all critical field points, and the resulting R vs T calibrations (one for each pressure) showed no systematic changes between calibrations. However, there was more scatter in the data above $0.8^{\circ}K$ than in

the first run, the RMS deviation from the fitted R vs. T curves being less than $0.0009^{\circ}K$ for each of the three calibrations. Hence, possible shifts in resistor calibration in the region above $0.8^{\circ}K$ were obscured by the scatter. Temperatures below $0.8^{\circ}K$ were calculated from the raw mutual inductance data without making use of the resistor calibrations. Above $0.8^{\circ}K$, temperatures were calculated from an R vs. T function obtained by fitting the data from all three calibrations to equation (75).

III. RESULTS AND DISCUSSION

A. Details of Magnetic Transitions

A transition which is typical of all transitions taken below $t^2 = 0.6$ is shown in Figure 6. The dashed line shows the transition shape corresponding to the demagnetizing factor calculated from the length to diameter ratio of the sample. All the transitions were somewhat narrower than would be predicted from the demagnetizing factor. This behavior has been observed before in aluminum by Cochran and Mapother,[41] and attributed to a large positive interphase surface free energy. Above $t^2 = 0.6$, superheating effects were observed. The transitions were very sharp and irregular in shape. However, the smoothness of the resulting critical field curves (see Figure 13) over the entire temperature range and the thermodynamic consistency of our data with calorimetric measurements of $\Delta C(T_c)$ (see Table 4) indicates that the critical field values obtained in the high temperature range must be very close (within about 0.1 gauss) to the equilibrium values.

Detailed measurements of supercooling were not made. During the first zero pressure run, the supercooled normal-to-superconducting transitions were about 16% lower than the corresponding superconducting-to-normal transitions. For all high pressure runs, and for the second zero pressure run, the supercooling was about 5% of H_c. It should be noted that the second zero pressure run was performed immediately after the 5400 and 7200 psi runs, without warming the sample above $15^{o}K$. The first zero pressure run

Figure 6. Typical superconducting transition. This transition was measured at T = 0.3259°K during the May 1966 3100 psi run.

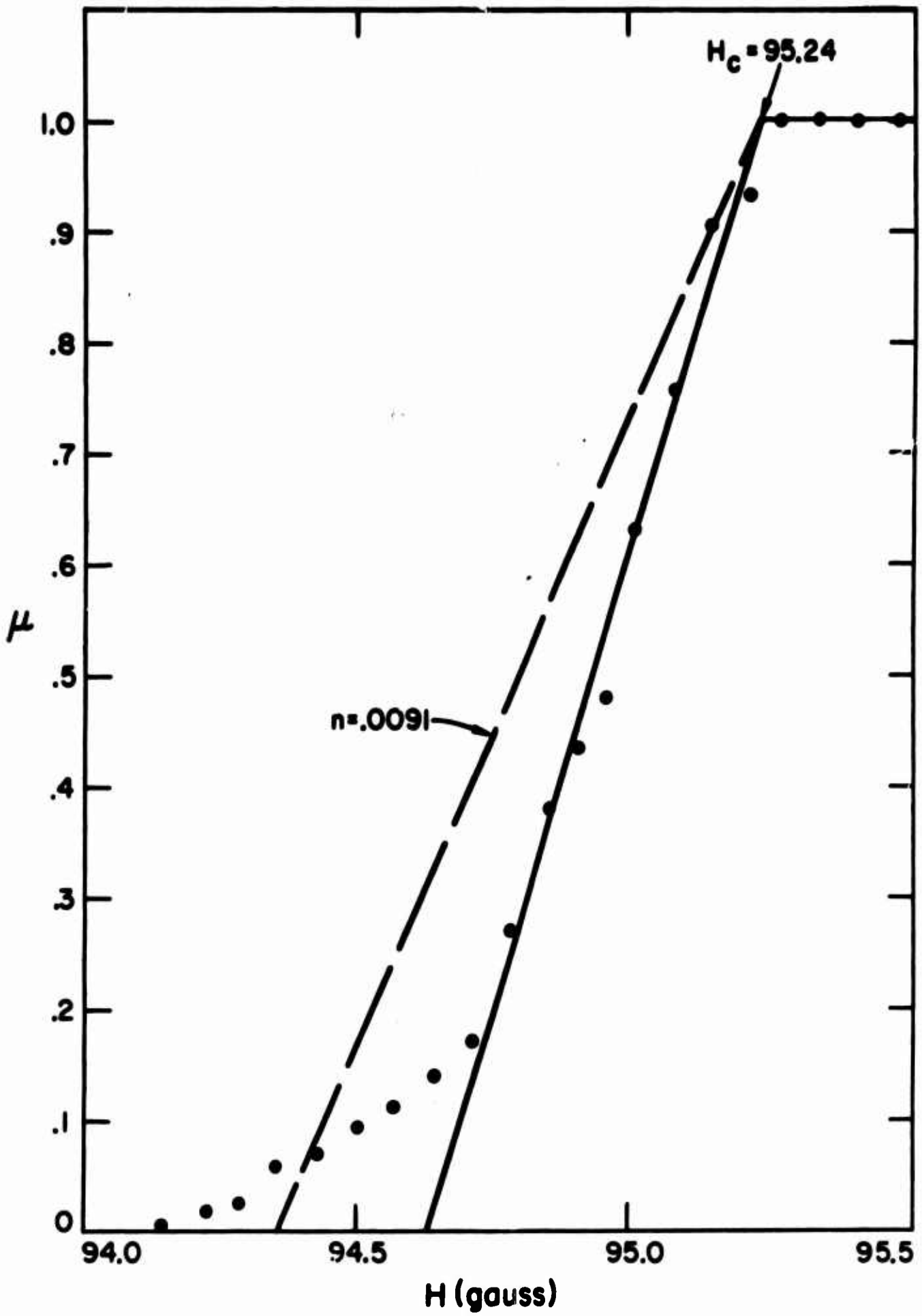
H_c = 95.24
n=.0091
1.0
.9
.8
.7
.6
.5
.4
.3
.2
.1
0
μ
94.0
94.5
95.0
95.5
H (gauss)

was made immediately after cooling down from room temperature. Although there was no broadening of the superconducting-to-normal transitions, it is possible that the pressure induced some permanent strain in the sample which reduced the supercooling. Any strains induced by application of high pressure prior to the first zero pressure run could possibly have annealed out at room temperature.

The critical field data are listed in Appendix B. The zero pressure listing includes the data from both zero pressure runs.

B. Analysis of Critical Field Curves

In Chapter I, Section C we showed that H_o and γ can be extracted directly from critical field data if a sufficient amount of data exist below $t = 0.25$. For aluminum, $T_c \approx 1.18^oK$; hence $t = 0.25$ corresponds to about $T = .295$, which is roughly the lowest temperature attainable with the He^3 refrigerator described here. Thus, to find H_o and γ, the critical field data must be fit to equation (22), using an assumed form for g(t), where

$$g(t) = \int_0^t (S_{es}/\gamma T_c)dt = \int_0^t \left\{ \int_0^t \left(\frac{C_{es}}{\gamma T_c}\right)\frac{dt}{t} \right\} dt \qquad (23)$$

as discussed in Chapter I. Phillips[68] found that in the range $0.3 \lesssim t \lesssim 0.5$, the superconducting electronic specific heat can be adequately represented by

$$(C_{es}/\gamma T_c) = 7.1\, e^{-1.34/t} \quad . \tag{76}$$

Phillips' result in this temperature range is in good agreement with earlier specific heat measurements by Goodman[69] and by Zavaritskii.[70] Using this form for $C_{es}/\gamma T_c$, we have fit the experimental data to equation (22) for $t < 0.5$, thus yielding values for H_o and γ at each pressure. We have assumed that $g(t)$ is independent of pressure, which is one of the assumptions used in the definition of simple similarity given in Section D of Chapter I. Values of T_c and $\left(\frac{\partial H_c(T_c)}{\partial T}\right)_P$ were obtained by extrapolating the data for $t^2 > 0.9$ to $H_c = 0$ using a straight-line fit in T^2. The energy gap at 0^oK was calculated from equation (27). The results are presented in Table 2. The error limits in Table 2 include the effects of absolute error estimates (see Appendix A) on the low-temperature and high-temperature extrapolations of the data and the uncertainty in the results due to data scatter. The effects of absolute error were found by performing the high-temperature and low-temperature extrapolations over again after adding the absolute error estimates of Appendix A to the measured H_c and T values. The uncertainty due to data scatter was estimated by observing the variation of H_o, γ, T_c, and $\left(\frac{\partial H_c(T_c)}{\partial T}\right)_P$ with the number of points used in the extrapolations. The error limits do not include the effects of possible errors in Phillips' specific heat results (equation (76)) or in the molar volume of aluminum. Let us now define a fiducial function

Table 2

PARAMETERS DEDUCED FROM CRITICAL FIELD CURVES*

Pressure (psi)	H_o (gauss)	γ (mj/mole $^oK^2$)	T_c (^oK)	$\frac{2\pi\gamma T_c^2}{VH_o^2}$	$\frac{2\Delta(o)}{kT_c}$	$\left(\frac{\partial H_c(T_c)}{\partial T}\right)_P$ (gauss/^oK)	$\Delta C(T_c)$ (mj/mole ^oK)
0	104.93±.2	1.349±.015	1.1793±.003	1.0846	3.48	-154±2	2.20±.06
3100	104.25±.2	1.337±.015	1.1732±.003	1.0780	3.49	-155±2	2.21±.06
5400	103.95±.2	1.341±.015	1.1701±.003	1.0827	3.49	-155±2	2.21±.06
7200	103.58±.2	1.343±.015	1.1659±.003	1.0842	3.48	-155±2	2.20±.06

*The molar volume of aluminum was taken to be 9.87 cc/mole[71] at zero pressure. At higher pressures this value was corrected, using for the compressibility $K_n = 1.34 \times 10^{-6}$ atm^{-1}.[49]

$$\bar{H}_c^2 = H_o^2 - \frac{4\pi\gamma}{V} T^2 \quad . \tag{77}$$

In Figure 7, we have plotted the deviation of H_c^2 from this fiducial function in units of H_o^2, using values of H_o, T_c, and γ from Table IV. From equation (22), this deviation is given by

$$\frac{H_c^2 - \bar{H}_c^2}{H_o^2} = \frac{8\pi\gamma T_c^2}{VH_o^2} g(t) \quad . \tag{78}$$

This plot shows the quality of the fit to g(t) as calculated from Phillips' measurements of the low-temperature superconducting electronic specific heat. Also shown is the curve calculated from BCS. If the BCS result for g(t) had been used to calculate H_o and γ, the resulting value of H_o would be about 0.1 gauss lower than that given in Table 2, and γ would be about 1% lower. Hence a 15% change in the assumed g(t) results in a 0.1% change in H_o and a 1% change in γ. Thus, the relaxation of the simple similarity restriction on g(t) to allow a mild pressure dependence would yield negligibly small changes in H_o.

The critical field curves are presented in Figure 8, in terms of their deviation from a fiducial parabola

$$D(t) = \frac{H_c}{H_o} - (1 - T^2/T_c^2), \tag{52}$$

using the values of H_o and T_c from Table 2. There is no significant pressure dependence of the shape of the deviation function, thus

Figure 7. Deviation of the critical field from $\bar{H}_c^2 = H_o^2 - (\frac{4\pi\gamma}{V})T^2$. Values for H_o, γ, and T_c used are those given in Table 2. Also plotted are the theoretical BCS curve and the curve calculated from Phillips' specific heat results, using equations (23) and (76).

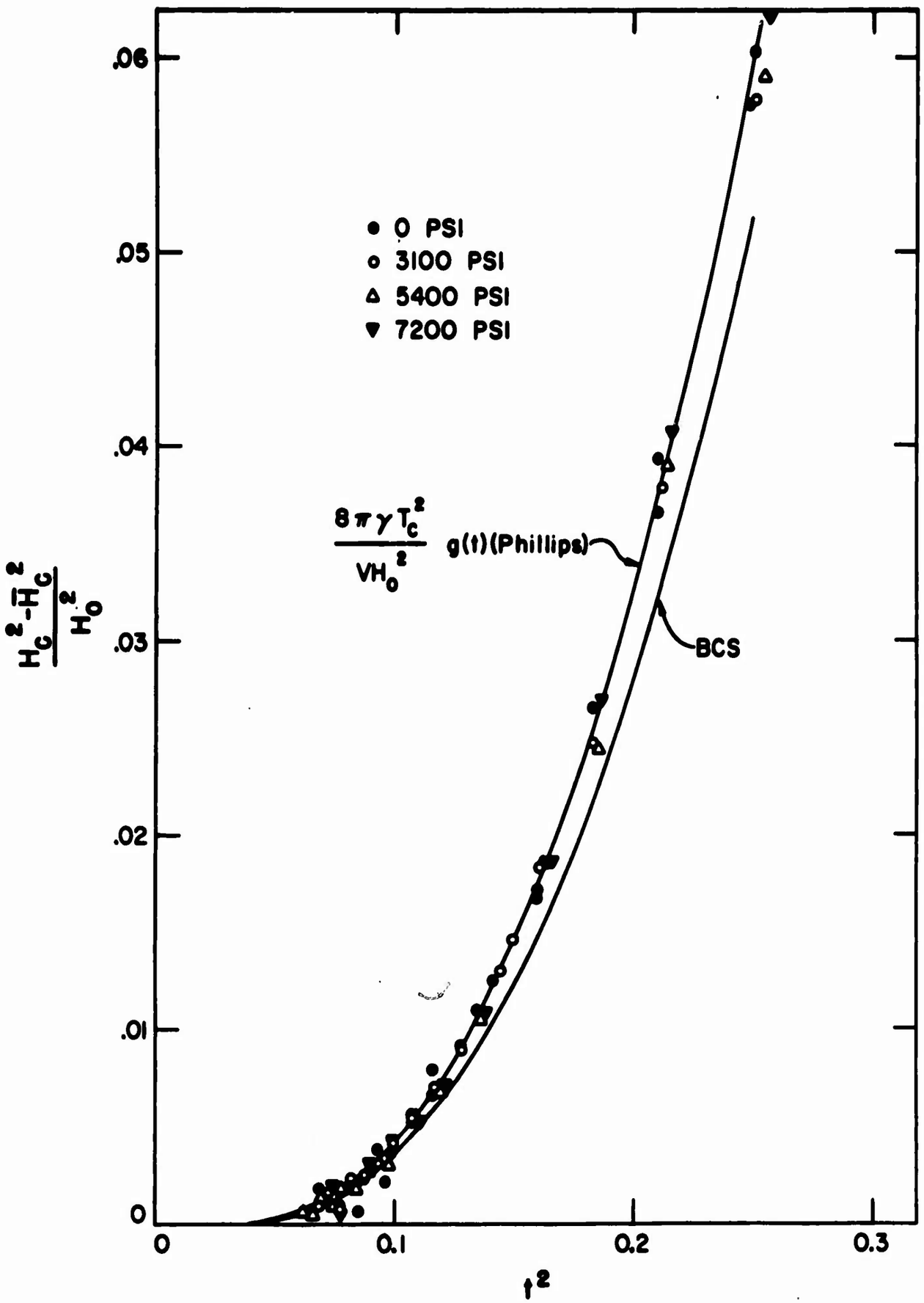
.06
.05
.04
.03
.02
.01
0
0
0.1
0.2
0.3
t²
$\frac{H_c^2 - \bar{H}_c^2}{H_0^2}$
● 0 PSI
○ 3100 PSI
△ 5400 PSI
▼ 7200 PSI
$\frac{8\pi\gamma T_c^2}{VH_0^2}$ g(t)(Phillips)
BCS

Figure 8. Experimental results for the deviation function $D(t) = H_c/H_o - 1 + T^2/T_c^2$ plotted versus the square of the reduced temperature, using H_o and T_c values from Table 2. The solid curve represents the theoretical BCS result. The dashed curve represents Phillips' specific heat results. Above $t^2 = .25$ the dashed curve was scaled from Figure 10 of Phillips' paper. Below $t^2 = .25$ it was calculated from Phillips' specific heat results using equations (22), (23), and (76).

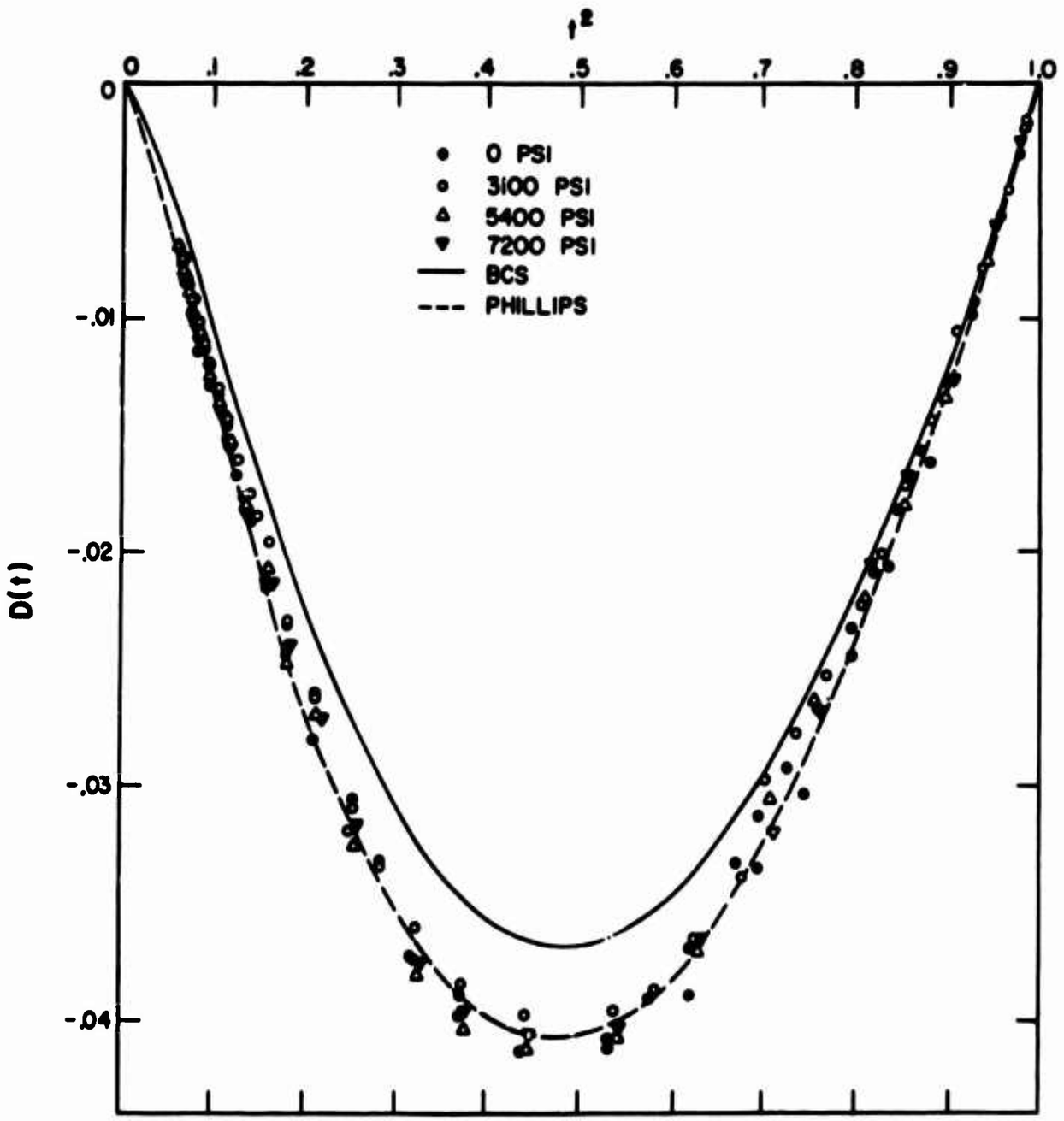
t²
0
.1
.2
.3
.4
.5
.6
.7
.8
.9
1.0
0
-.01
-.02
-.03
-.04
D(t)
0 PSI
3100 PSI
5400 PSI
7200 PSI
BCS
PHILLIPS

verifying the principle of simple similarity for these critical field curves. Note that if the BCS g(t) had been used to find H_o, the deviation functions would have been shifted up by only 0.0005 at $t^2 = 0.5$. They still would be in much better agreement with Phillips' results than with the deviation function calculated from BCS.

ΔS was calculated from equation (13), where the derivative dH_c/dT was evaluated at each point by fitting a few points in the neighborhood of a given point to $H_c = a + bT^2$. In most cases, three points on either side of the point in question were used. S_{es} was then obtained from equation (17), and in Figure 9 $S_{es}/\gamma T_c$ is displayed for all the data. The $S_{es}/\gamma T_c$ curves are nearly identical for all pressures, and lie slightly above the BCS curve.

C. Effect of Pressure on Critical Field Curves

In the previous section, we found H_o, T_c, and γ as a function of pressure (see Table 2) by low-temperature and high-temperature extrapolations of the data, and the critical field curves were shown to obey simple similarity. In this section, starting from simple similarity, we will find dH_o/dP, $\left(\frac{\partial H_c(T_c)}{\partial P}\right)_T$, and $(d\ln\gamma/d\ln V)$ by using equations (64) and (65) developed in Chapter I, Section C. We will fit $\Delta H_c(P,t^2)$ to a smooth curve in t^2 over the entire temperature range by assuming a form for $(\partial H_c/\partial P)_T$. This method should reduce scatter in the pressure variation of H_o, T_c, and γ, since these quantities will not depend upon extrapolations which use only a small fraction of the data.

Figure 9. Superconducting electronic entropy calculated from the experimental data (see text), using values of γ and T_c from Table 2. Each point plotted below t = .38 represents the average of 4 entropy points calculated from the data. In the inset, the portion of the graph below t = .38 is enlarged, showing all the entropy points. Also plotted is the theoretical BCS curve.

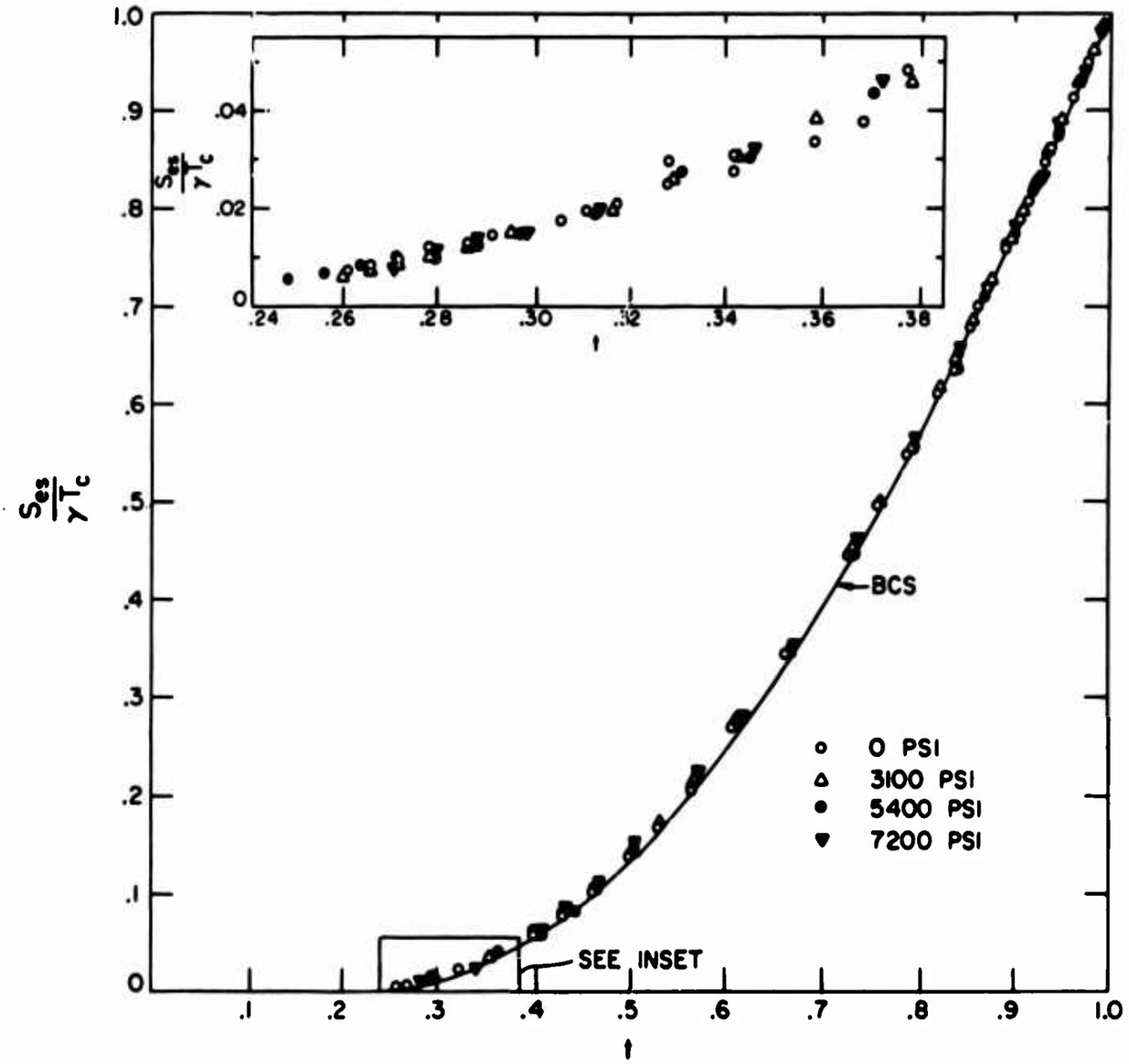
$\frac{S_{es}}{\gamma T_c}$
t
BCS
SEE INSET
0 PSI
3100 PSI
5400 PSI
7200 PSI

Figure 10 displays the zero pressure data and a curve which was fit to the data in least squares fashion. This function is (using $T_c = 1.1793\,^{\circ}K$)

$$H_c = \sum_{i=0}^{6} a_i (t^2)^i$$

where

$$a_0 = 105.19795$$

$$a_1 = -121.47833$$

$$a_2 = -1.4105433$$

$$a_3 = 57.608482 \qquad (79)$$

$$a_4 = -63.221601$$

$$a_5 = 25.785877$$

$$a_6 = -2.5004711$$

for $0.06 \leq t^2 \leq 1.0$.

In Figure 11, the difference $\Delta H_c = H_c(P,T) - H_c(0,T)$, where $H_c(0,T)$ is calculated from equation (79), is plotted versus $(T/T_c(P))^2$. According to simple similarity, via equation (65),

$$\Delta H_c(P,t^2) = \Delta H_o(P)\left[1 + \left(2\,\frac{d\ln T_c/dP}{d\ln H_o/dP} - 1\right)t^2 + D(t) - 2t^2\,\frac{\partial D}{\partial t^2}\,\frac{d\ln T_c/dP}{d\ln H_o/dP}\right]. \qquad (80)$$

The last two terms introduce some curvature into $\Delta H_c(P,t^2)$. The exact shape of (80) depends upon the end points at $t^2 = 0$ and 1, through

Figure 10. Zero pressure results for the deviation function. The error bars are estimates of the limit of relative error (see Appendix A). The solid curve is a polynomial function (equation (79)) which is a best least-squares fit to the data.

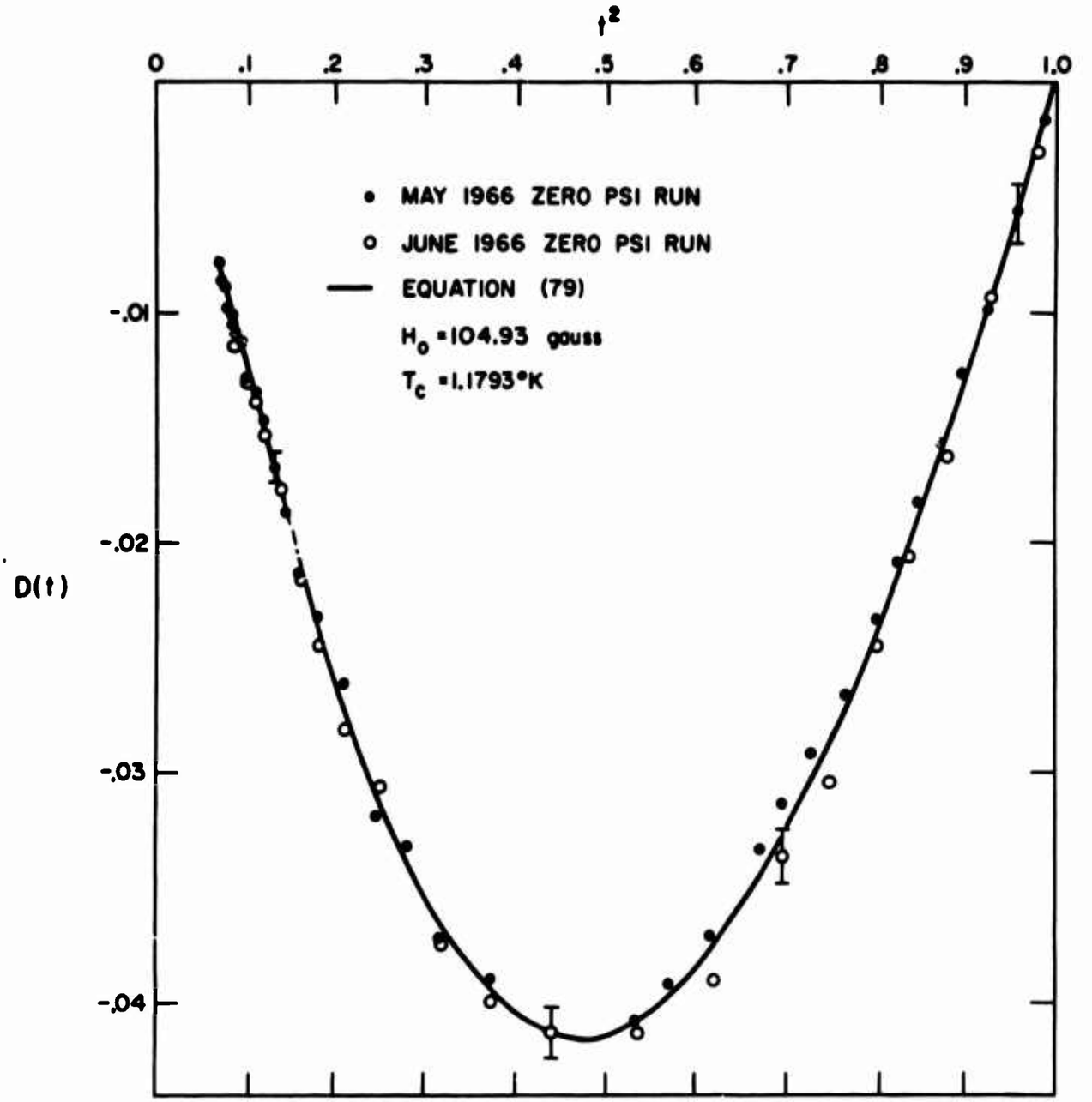
t²
0
.1
.2
.3
.4
.5
.6
.7
.8
.9
1.0
D(t)
-.01
-.02
-.03
-.04
• MAY 1966 ZERO PSI RUN
○ JUNE 1966 ZERO PSI RUN
— EQUATION (79)
H₀ = 104.93 gauss
T_c = 1.1793°K

Figure 11. The pressure shift of the critical field defined by $\Delta H_c(P,T) = H_c(P,T) - H_c(0,T)$, where $H_c(0,T)$ is given by equation (79), is plotted versus the square of the reduced temperature. The values of T_c at each pressure are taken from Table 2. The error bars are estimates of the limit of relative error (see Appendix A). The solid curves represent the best least-squares fit to the data assuming simple similarity (see text).

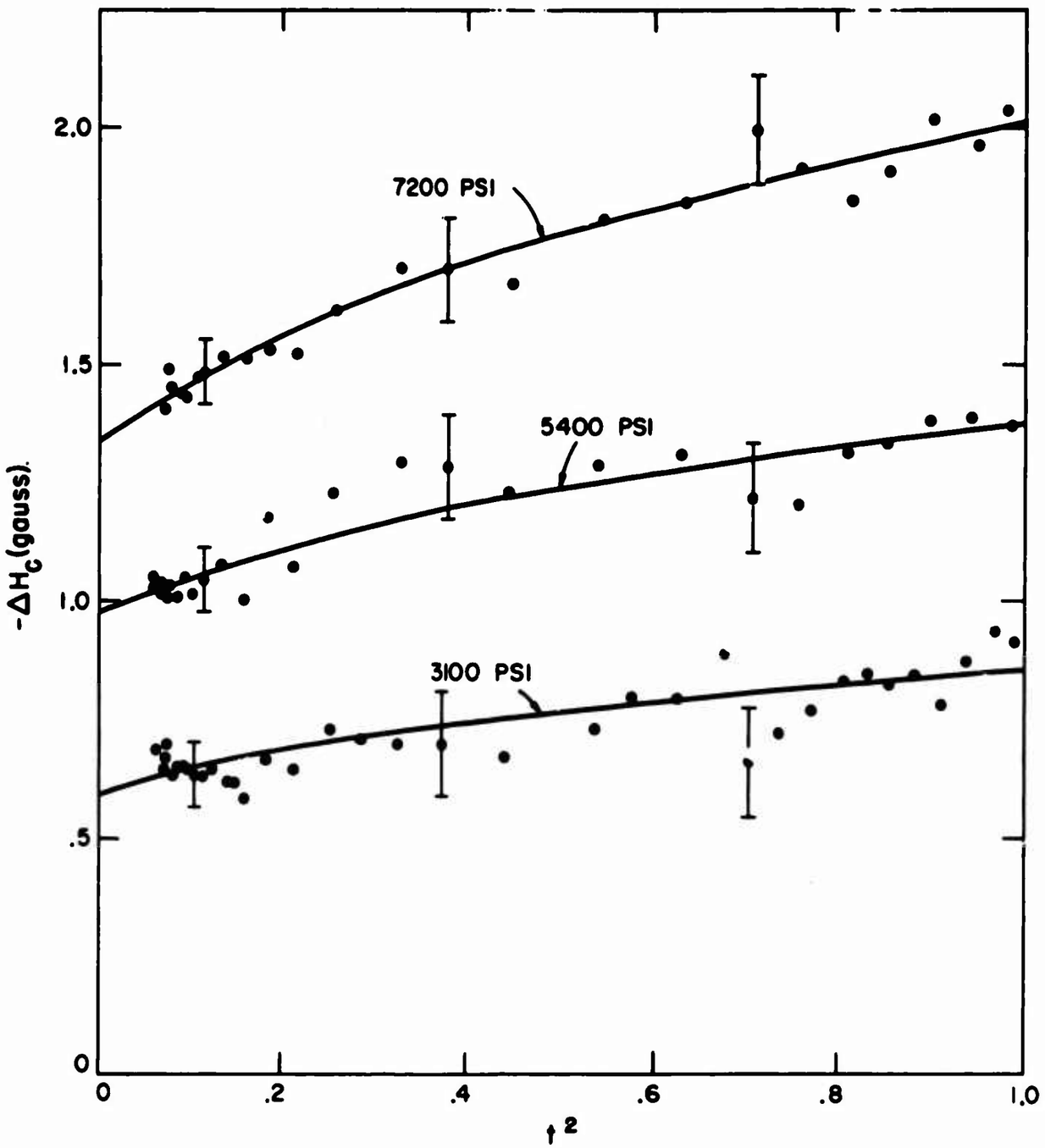
7200 PSI
5400 PSI
3100 PSI
$-\Delta H_c$ (gauss)
t^2
2.0
1.5
1.0
.5
0
0
.2
.4
.6
.8
1.0

the factor $(d\ln T_c/dP)/(d\ln H_o/dP)$. The end points of (80) are given by

$$\left.\begin{aligned} \frac{\Delta H_c(P,0)}{\Delta H_o(P)} &= 1 \quad , \; t^2 = 0 \\ \frac{\Delta H_c(P,T_c)}{\Delta H_o(P)} &= 2\,\frac{d\ln T_c/dP}{d\ln H_o/dP}\left(1 - \left(\frac{\partial D}{\partial t^2}\right)_{T_c}\right) \quad , \; t^2 = 1 \end{aligned}\right\} . \tag{81}$$

The procedure used to find the best simple similarity fit to the ΔH_c data was as follows. Let us define a function given by

$$u(t^2) = 1 + \left\{2\,\frac{d\ln T_c/dP}{d\ln H_o/dP}\left(1 - \left(\frac{\partial D}{\partial t^2}\right)_{T_c}\right) - 1\right\} t^2 . \tag{82}$$

This function is a straight line in t^2 passing through the end points of (80). Thus we may define a parameter t^* such that

$$1 + \left[2\,\frac{d\ln T_c/dP}{d\ln H_o/dP}\left(1 - \left(\frac{\partial D}{\partial t^2}\right)_{T_c}\right) - 1\right] t^{*2} = \tag{83}$$

$$1 + \left[2\,\frac{d\ln T_c/dP}{d\ln H_o/dP} - 1\right] t^2 + D(t) - 2t^2\,\frac{\partial D}{\partial t^2}\,\frac{d\ln T_c/dP}{d\ln H_o/dP} .$$

Thus the simple similarity function (80), which is curved in t^2, is a straight line in t^{*2}. The dependence of t^{*2} on t^2 depends upon the shape of D(t) and the value of $\dfrac{d\ln T_c/dP}{d\ln H_o/dP}$. The functional form of D(t) can be determined from (79). We then evaluate t^{*2} versus t^2 by

by estimating $\frac{d\ln T_c/dP}{d\ln H_o/dP}$ on the basis of a straight-line fit of $\Delta H_c(P,t^2)$ versus t^2. The ΔH_c data were then fit in least-squares fashion to a straight line in t^{*2}, yielding a new set of end points. These new end points could be used to make a better estimate of $\frac{d\ln T_c/dP}{d\ln H_o/dP}$ for finding t^{*2}. We found that carrying this procedure beyond one iteration produced negligible changes in the end points. The solid curves in Figure 11 are the best simple similarity fits to the data. The results may be expressed as follows:

$$\left.\begin{aligned} \Delta H_c(3100\ \text{psi}) &= -\left[(0.589 \pm .016) + (.261 \pm .027)t^{*2}\right] \\ \Delta H_c(5400\ \text{psi}) &= -\left[(0.979 \pm .018) + (.401 \pm .034)t^{*2}\right] \\ \Delta H_c(7200\ \text{psi}) &= -\left[(1.335 \pm .018) + (.672 \pm .029)t^{*2}\right] \end{aligned}\right\} . \quad (84)$$

The errors in the coefficients are standard deviations computed from least-squares analysis formulae.[72] In Table 3 the values of ΔH_o and $\Delta H_c(P,T_c)$ computed from (84) for each pressure are listed. Note that $\Delta H_c(P,T_c)$ and ΔT_c are related by equation (63).

$$\Delta H_c(P,T_c) = -\Delta T_c(P)\left(\frac{\partial H_c(T_c)}{\partial T}\right)_P \quad (85)$$

Also tabulated in Table 3 are values taken from Table 2, Section B. The values for the end points calculated from simple similarity are in good agreement with the calculations of Section B for the 5400 and 7200 psi data; the agreement for the 3100 psi data is not as good.

Table 3

PRESSURE SHIFT OF THE END POINTS OF THE CRITICAL FIELD CURVE

Pressure (psi)	Results from simple similarity analysis*			Results from direct analysis of individual critical field curves†		
	ΔH_o (gauss)	$\Delta H_c(P,T_c)$ (gauss)	ΔT_c (°K)	ΔH_o (gauss)	$\Delta H_c(P,T_c)$ (gauss)	ΔT_c (°K)
3100	$-.589 \pm .016$	$-.850 \pm .043$	-.0055	-.68	-.94	-.0061
5400	$-.979 \pm .018$	$-1.380 \pm .052$	-.0090	-.98	-1.42	-.0092
7200	$-1.335 \pm .018$	$-2.007 \pm .047$	-.0130	-1.35	-2.07	-.0134

*Calculated from (83), using (84) to find ΔT_c, with $\frac{dH_c(T_c)}{dT} = -154.$

†Calculated from Table 2, using (84) to find $\Delta H_c(P,T_c)$ with $\frac{dH_c(T_c)}{dT} = -154.$

The end points calculated from simple similarity are plotted in Figure 12, from which values for $\frac{dH_o}{dP}$ and $\left(\frac{\partial H_c(T_c)}{\partial P}\right)_T$ have been extracted by fitting the points to straight lines in least-squares fashion. We find

$$\frac{dH_o}{dP} = -(2.70 \pm .06) \times 10^{-3} \text{ gauss/atm.}$$
$$\left(\frac{dH_c(T_c)}{\partial P}\right)_T = -(4.01 \pm .2) \times 10^{-3} \text{ gauss/atm.} \tag{86}$$

Again, the error bars denote standard deviations computed from least-squares analysis formulae.[72] $\frac{d\ln\gamma}{d\ln V}$ may be calculated from (64) using the values of H_o, T_c, and $\left(\frac{\partial H_c(T_c)}{\partial T}\right)_P$ from our zero pressure results. Rewriting (64), we find

$$\frac{d\ln\gamma}{d\ln V} = 1 - 2\left[\frac{(dH_o/dP)}{K_n H_o} + \frac{(\partial H_c(T_c)/\partial P)_T}{K_n T_c (\partial H_c(T_c)/\partial T)_P}\right]. \tag{87}$$

Using for the isothermal compressibility[49]

$$-\left(\frac{\partial \ln V}{\partial P}\right)_T = K_n = 1.34 \times 10^6 \text{ atm}^{-1}, \tag{88}$$

this gives

$$\frac{d\ln\gamma}{d\ln V} = 6.45 \pm 3. \tag{89}$$

The uncertainty given in (89) does not reflect any possible errors in the compressibility value, but contains the uncertainties in H_o, T_c,

Figure 12. The pressure shifts at T=0 and T = $T_c(P)$ are plotted versus pressure. These pressure shifts are the end points of the solid curves in Figure 11, and are tabulated in Table 3. The fact that each $\Delta H_c(T_c)$ is evaluated at $T_c(P)$ instead of $T_c(0)$, for instance, makes negligible difference (less than .01 gauss) in each case. The solid lines represent the best least-squares fit straight lines.

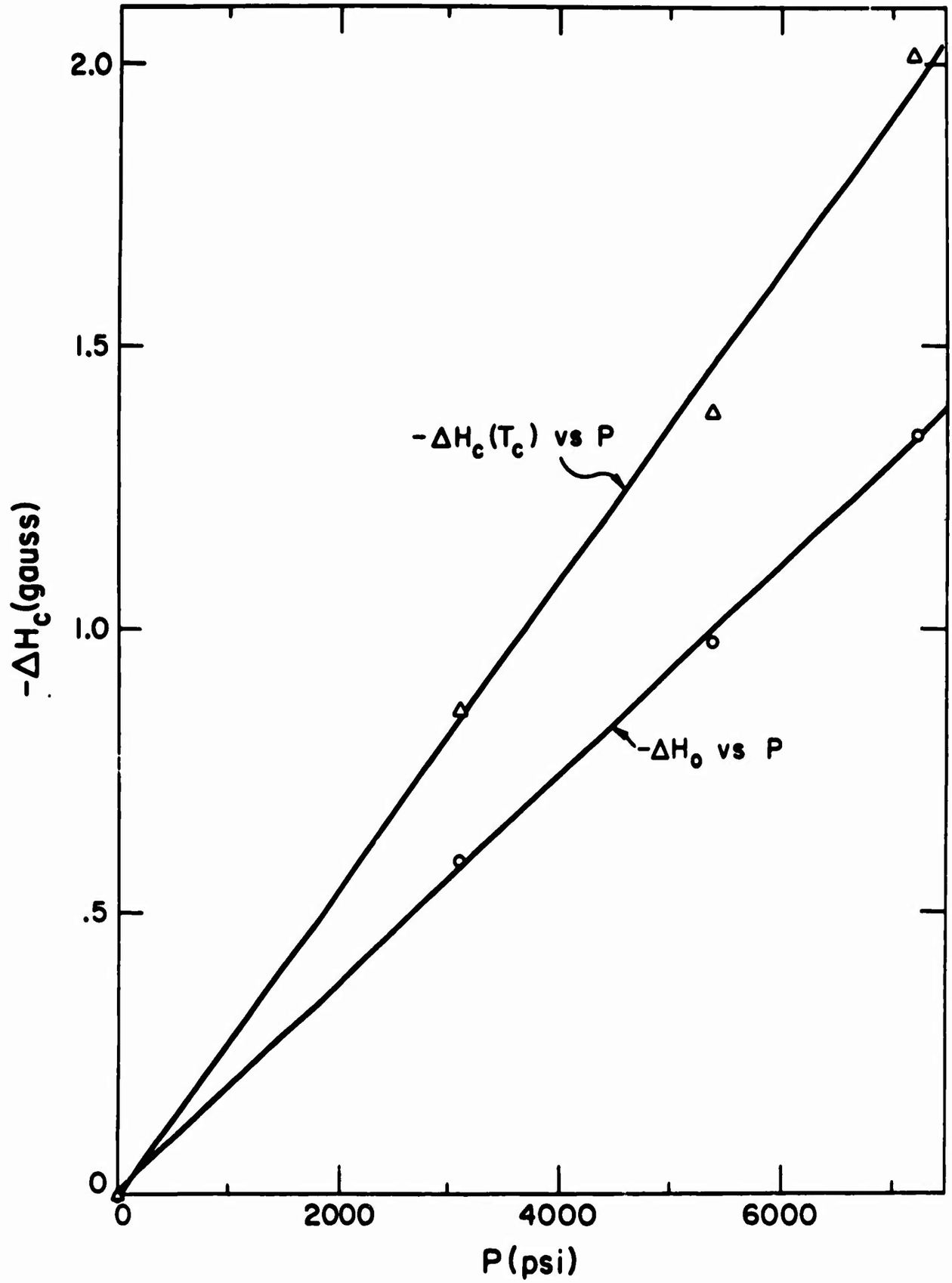
2.0
1.5
1.0
.5
0
0
2000
4000
6000
P(psi)
$-\Delta H_c$(gauss)
$-\Delta H_c(T_c)$ vs P
$-\Delta H_0$ vs P

and $\left(\frac{\partial H_c(T_c)}{\partial T}\right)_P$ listed in Table 2 and the uncertainties in $\frac{dH_o}{dP}$ and $\left(\frac{\partial H_c(T_c)}{\partial P}\right)_T$ given in (86).

We may also calculate the volume dependence of the BCS coupling constant from (69):

$$\frac{d\ln A}{d\ln V} = N(o)A\left[\frac{d\ln T_c}{d\ln V} - \frac{d\ln\theta_D}{d\ln V}\right] + 1 - \frac{d\ln\gamma}{d\ln V} \quad . \tag{69}$$

First we must find N(o)A, $\frac{d\ln\theta_D}{d\ln V}$, and $\frac{d\ln T_c}{d\ln V}$. $\frac{d\ln T_c}{d\ln V}$ is given by

$$\frac{d\ln T_c}{d\ln V} = \frac{(\partial H_c(T_c)/\partial P)_T}{K_n T_c (\partial H_c(T_c)/\partial T)_P} = 16.5 \pm 1.1 \quad . \tag{90}$$

White[54] has measured the thermal expansion of aluminum at low temperatures. From his results, using equation (43),

$$\frac{d\ln\theta_D}{d\ln V} = -2.25 \pm .2 \tag{91}$$

where we have used $\theta_D = 427.7^oK$.[68] N(o)A may be calculated from (67). Using $T_c = 1.1793^oK$ and $\theta_D = 427.7^oK$, this yields

$$N(o)A = 0.167. \tag{92}$$

Substituting into (69),

$$\frac{d\ln A}{d\ln V} = .167\left[\frac{d\ln T_c}{d\ln V} + 2.25 \pm .2\right] + 1 - \frac{d\ln\gamma}{d\ln V} \quad . \tag{93}$$

For our results, we find

$$\frac{d\ln A}{d\ln V} = -2.3 \pm 3 \qquad (94)$$

D. Comparison with Other Results

The agreement of our zero pressure measurements with previous results can be seen by comparing our parameters listed in Table 4 with the data of Phillips,[68] Rorer et al.,[40] and Hopkins[39] listed there also. The results of our magnetic measurements are thermodynamically consistent with calorimetric results. The degree of consistency can be seen by observing (Figure 7) that our deviation function, D(t), is practically identical to that calculated from Phillips' data using the equations of Chapter I. The only discrepancies between our data and that of Phillips are in the values of H_o and T_c. His results for these quantities differ from ours by about 1 to 2%. Although our values of H_o and T_c agree with those of Caplan and Chanin,[42] our results for D(t) differ markedly from theirs at low temperatures. Our data are displayed with theirs in Figure 13. They attribute the large scatter in their low temperature data to their temperature measurements using He^3 vapor pressure thermometry. Below 0.5°K precise He^3 vapor pressure measurements are very difficult to make, due to the smallness of the pressure and the large thermomolecular corrections which must be made. Also, as they state in their paper, there is question as to whether their method

Table 4

ALUMINUM DATA (ZERO PRESSURE)

Reference	H_o (gauss)	T_c (^oK)	γ (mj/mole$^oK^2$)	$\frac{2\pi\gamma T_c^2}{VH_o^2}$	$\left(\frac{\partial H_c(T_c)}{\partial T}\right)_P$ (gauss/^oK)	cal. $\Delta C(T_c)$ mj/mole^oK	mag. $\Delta C(T_c)$ $\frac{mj}{mole^oK}$
Goodman and Mendoza[74]	106	1.197±.01					
Faber[75]	96±1	1.172±.003			-164		2.43
Cochran and Mapother[41]	99±1	1.196±.005			-165.5		2.57
Caplan and Chanin[42]	104.8±.6	1.175±.001	1.23-1.30	1.061	-158±4		2.31±.12
Rorer et al.[40]		1.173-1.188			-153	2.21	2.19±.03
Hopkins and Mapother[3c]		1.1797±.0003			-152	2.21	2.14
Phillips[68]	103.0	1.163	1.35±.01	1.088	-152	2.10	
This work (Zero pressure)	104.93±.2	1.1793±.003	1.349±.015	1.085	-154±2		2.20±.06

Figure 13. The deviation function $D(t) = H_c/H_o - 1 + T^2/T_c^2$ is plotted using values for H_o and T_c at zero pressure from Table 2. Values for H_o and T_c at non-zero pressure were calculated using the zero pressure values in Table 2 and the pressure shifts in Table 3 calculated from simple similarity. Points at all pressures are plotted with the same symbol. Also plotted are the data of Caplan and Chanin using our zero pressure H_o and T_c. The theoretical calculation of Clem assuming $\langle a^2 \rangle = .01$ is represented by the solid curve.

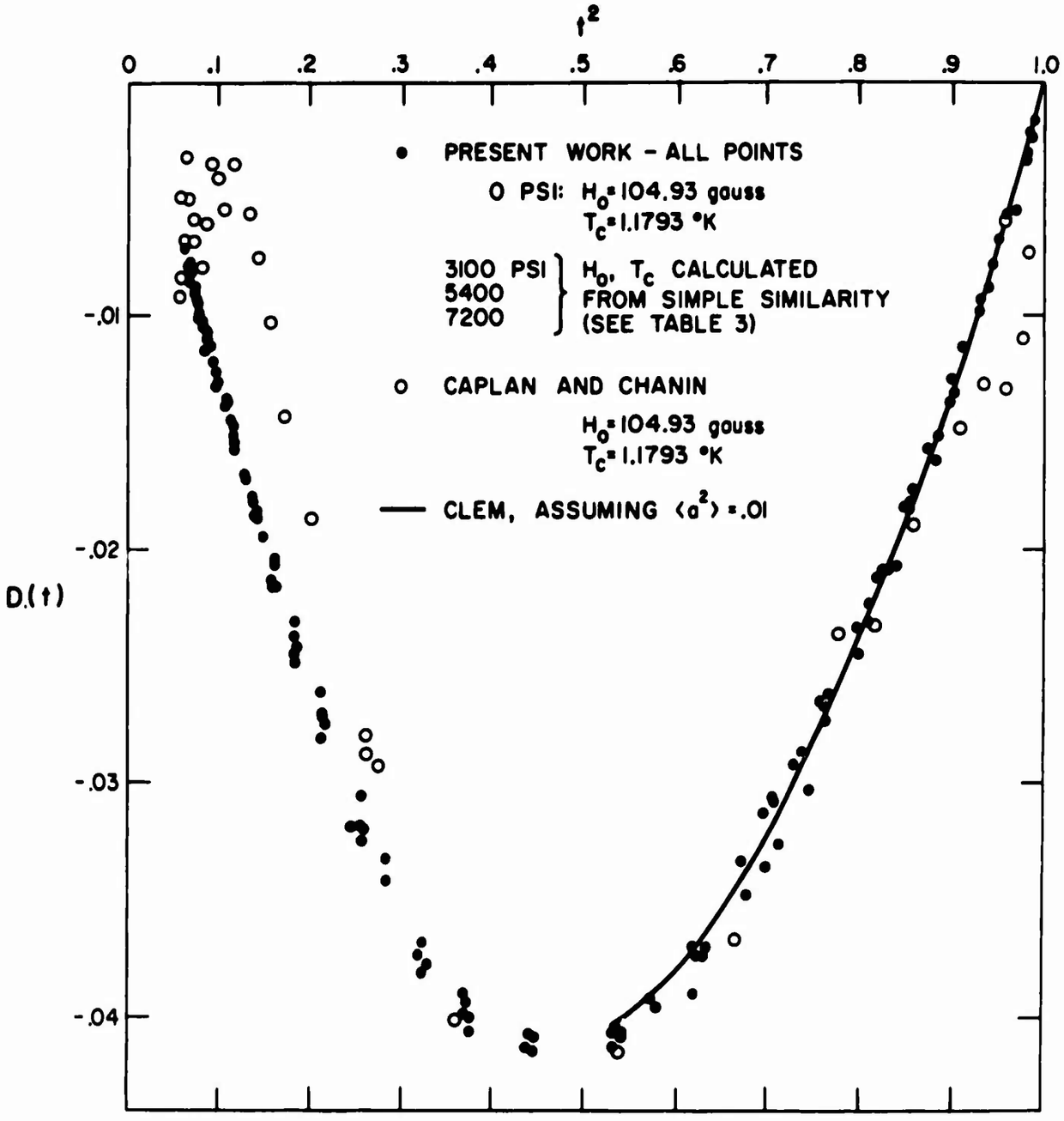
t^2
0
.1
.2
.3
.4
.5
.6
.7
.8
.9
1.0
-.01
-.02
-.03
-.04
D.(t)
PRESENT WORK - ALL POINTS
0 PSI: H_0=104.93 gauss
T_c=1.1793 °K
3100 PSI
5400
7200
H_0, T_c CALCULATED FROM SIMPLE SIMILARITY (SEE TABLE 3)
CAPLAN AND CHANIN
H_0=104.93 gauss
T_c=1.1793 °K
CLEM, ASSUMING $\langle a^2 \rangle$ = .01

of measuring H_c gives thermodynamic equilibrium values. Their method involves superimposing a field gradient upon a DC field of about H_c, thus creating a normal-superconducting phase boundary in the sample. The position of the boundary is monitored as the DC field is changed by monitoring in a set of pickup coils the signal induced by a small 10 cps modulation field. The value of the applied DC field for which the phase boundary reaches a position in the sample such that the gradient field is zero is taken to be H_c. Caplan and Chanin mention that if the phase boundary is not free to move in the sample, perhaps due to pinning by dislocations, the H_c values obtained might not correspond to thermodynamic equilibrium.

In Figure 14, our high temperature zero pressure data are plotted on the same graph with the data of Hopkins, which were taken on a large spherical single crystal. The agreement of our data with Hopkins' data is excellent.

It is also of interest to compare experimental results for the energy gap at $0^{\circ}K$ in aluminum with values calculated from our results using theoretical equations. Such a comparison is made in Table 5. The pertinent BCS equation is

$$\frac{VH_o^2}{2\pi\gamma T_c^2} = \frac{3}{4\pi^2}\left(\frac{2\Delta(o)}{kT_c}\right)^2 \quad . \tag{95}$$

The BCS result for the energy gap at $0^{\circ}K$ is

$$\frac{2\Delta(o)}{kT_c} = 3.528 \quad . \tag{96}$$

Figure 14. Our zero pressure data near T_c and the data of Hopkins are plotted versus T^2. The solid line has a slope of -154 gauss/^oK at T_c = 1.1793^oK.

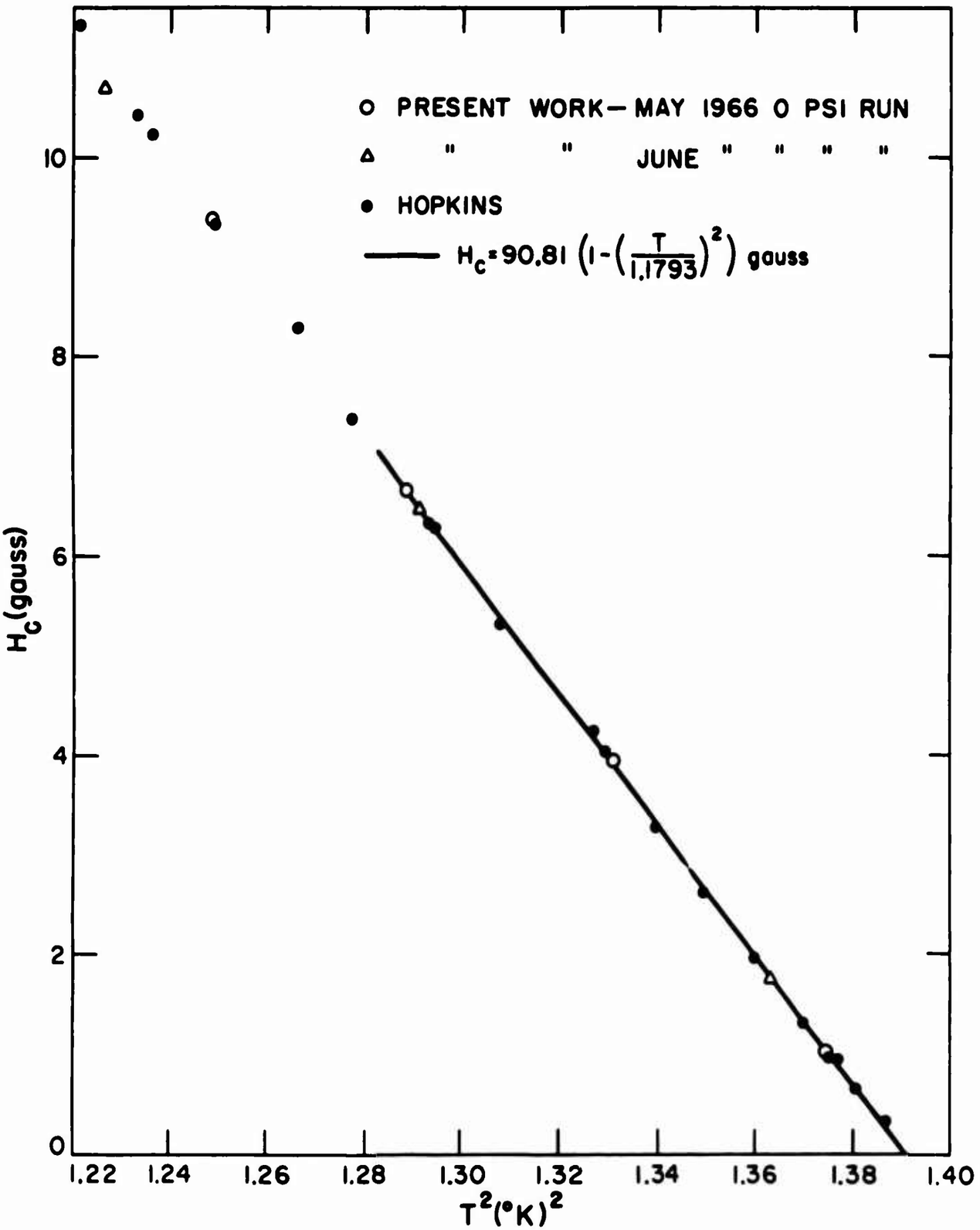
o PRESENT WORK— MAY 1966 0 PSI RUN
Δ " " JUNE " " " "
• HOPKINS
$H_c = 90.81\left(1-\left(\frac{T}{1.1793}\right)^2\right)$ gauss
H_c (gauss)
0
2
4
6
8
10
1.22
1.24
1.26
1.28
1.30
1.32
1.34
1.36
1.38
1.40
$T^2(°K)^2$

Table 5

ENERGY GAP VALUES

	$\frac{2\Delta(o)}{kT_c}$	Method
Present work	$3.48 \pm .02$	Equation (95)
Present work	$3.45 \pm .02$	Equation (97), with $\langle a^2 \rangle = .01$
Biondi, Garfinkel, Thompson[76]	$3.04 - 3.50 \pm .05$	Surface resistance (single crystal)
Biondi and Garfunkel[77]	$3.25 \pm .1$	Surface resistance (polycrystal)
David and Poulis[78]	$3.7 \pm .3$	Ultrasonic attenuation
Zavaritskii[79]	$3.37 \pm .1$	Tunneling
Douglass and Meservey[80]	$3.1 - 3.4$	Tunneling
Giaever and Megerle[81]	4.2 ± 0.6	Tunneling
Shapiro et al.[82]	$2.5 \pm .3$	Tunneling
Masuda and Redfield[83]	3.2	Nuclear spin relaxation time
BCS[15]	3.528	Equation (96)
Clem[73]	3.48	Equation (98) with $\langle a^2 \rangle = .01$

The BCS relations are based on the assumption that the electron-phonon interaction responsible for superconductivity is isotropic in momentum space. Clem[73] has calculated the effects of anisotropy on the superconducting energy gap and the thermodynamic properties of superconductors. His calculation of anisotropy effects leads to the following modifications in (95) and (96).

$$\frac{VH_o^2}{2\pi\gamma T_c^2} = \frac{3}{4\pi^2}\left(\frac{2\Delta(o)}{kT_c}\right)^2 (1 + \langle a^2\rangle) \tag{97}$$

$$\frac{2\Delta(o)}{kT_c} = 3.528\ (1 - \tfrac{3}{2}\langle a^2\rangle) \tag{98}$$

where $\langle a^2\rangle$ is the mean-squared anisotropy; it is the Fermi-surface average of the square of the deviation of the energy gap parameter from its average value. Masuda and Redfield[83] found that their nuclear spin relaxation measurements in aluminum were consistent with an energy gap of $3.2kT_c$ smeared by about 10%. The data of Biondi, Garfunkel, and Thompson[76] indicate that there may be two distinct gaps in aluminum, separated by about $0.4kT_c$, possibly due to anisotropy. Markowitz and Kadanoff[89] estimate that $\langle a^2\rangle = .01$ for aluminum, on the basis of measurements of the critical temperature versus impurity doping by Chanin et al.[90]. For this reason, we have included in Table 5 calculations using Clem's formulae, assuming $\langle a^2\rangle = 0.01$. Also included in Figure 13 is Clem's result for D(t), assuming $\langle a^2\rangle = 0.01$.

The variations between the various results for $\left(\frac{2\Delta(o)}{kT_c}\right)$ listed in Table 5 may be partially due to the methods of interpretation of experimental data. The values from surface resistance (microwave absorption) experiments were found by measuring the photon energy corresponding to the onset of absorption, which is characterized by a change in slope of a plot of surface resistance versus frequency. The change in slope takes place over a range of frequencies; hence the observer must select a criterion for deciding what frequency corresponds to the energy gap. Values found from nuclear spin relaxation and ultrasonic attenuation experiments depend upon the validity of theoretical equations used in the data analysis, and our results are subject to the same limitation. Variations in the results from tunneling experiments, on the other hand, may be due to problems in making good thin-film samples. Douglass and Meservy found variations of about 10% in $\left(\frac{2\Delta(o)}{kT_c}\right)$ from sample to sample which they tentatively attributed to sample imperfections such as strains or impurities.

Our pressure effect results are listed with those of other workers in Table 6. The values for $\frac{dH_o}{dP}$ and $\left(\frac{\partial H_c(T_c)}{\partial P}\right)_T$ listed for Olsen[50] and Gross and Olsen[51] were extracted by them from their experimental data on the basis of simple similarity, ignoring the deviation of the critical field curve from a parabola. That is, they fit their data to $\Delta H_c = a + bt^2$. Such an analysis leads to values of $\frac{dH_o}{dP}$ and $\left(\frac{\partial H_c(T_c)}{\partial P}\right)_T$ which are perhaps 5 percent higher than one would obtain by including the deviation from parabolicity

of $H_c(T)$ as determined in this experiment, as we did in our simple similarity analysis. The value of the ratio $(dH_o/dP)\Big/\left(\frac{\partial H_c(T_c)}{\partial P}\right)_T$, which enters the calculation of $\frac{d\ln\gamma}{d\ln V}$ (see equation (64)) is probably affected by 1 or 2 percent. The value of $\frac{d\ln\gamma}{d\ln V}$ listed for Gross and Olsen is not the value given in their paper. It is a value calculated from their values of $\frac{dH_o}{dP}$ and $\left(\frac{\partial H_c(T_c)}{\partial P}\right)_T$ and our values of H_o, T_c, $\left(\frac{\partial H_c(T_c)}{\partial T}\right)_P$, and K_n, via equation (87). Considering the experimental uncertainties and differences in the methods of analysis, our values of $\frac{dH_o}{dP}$, $\left(\frac{\partial H_c(T_c)}{\partial P}\right)_T$, and $\frac{d\ln\gamma}{d\ln V}$ are in reasonable agreement with the results of Gross and Olsen, and, except for $\left(\frac{\partial H_c(T_c)}{\partial P}\right)_T$, in disagreement with the earlier work of Olsen. Both our value of $\frac{d\ln\gamma}{d\ln V}$ and that calculated from Gross and Olsen's work disagree with the values calculated from thermal expansion data listed in Table 6. It should be mentioned that thermal expansion measurements give $\frac{d\ln\gamma}{d\ln V}$ directly via equation (42), while in the absence of sufficient critical field data below $t = .25$ $\frac{d\ln\gamma}{d\ln V}$ must be inferred from simple similarity analysis of the critical field data (equation (87)). The two terms in brackets in (87) are of nearly the same magnitude and opposite sign; hence the resulting value of $\frac{d\ln\gamma}{d\ln V}$ is quite susceptible to error. A better determination of $\frac{d\ln\gamma}{d\ln V}$ from critical field data must await the extension of precise measurements to higher pressures and much lower temperatures where the data can be analyzed to give $\frac{d\ln\gamma}{d\ln V}$ directly, using equation (44).

Table 6

PRESSURE EFFECT RESULTS

	$\left(\frac{\partial H_o}{dP}\right)$ gauss/atm.	$\left(\frac{\partial H_c}{\partial P}\right)_{T_c}$ gauss/atm.	$\frac{\beta_{en}}{T}$ $^oK^{-2}$	$\frac{\beta_{gn}}{T^3}$ $^oK^{-4}$	$\frac{d\ln\gamma}{d\ln V}$	$\frac{d\ln A}{d\ln V}$	$\left(-\frac{\Gamma_G}{d\ln\theta}{d\ln V}\right)$
Muench[84]		-3.3×10^{-3}					
Olsen[50]	-11.5×10^{-3}	-4.0×10^{-3}			130±60		
Gross and Olsen[51]	$(-3.1\pm.2)\times10^{-3}$	$(-4.8\pm.4)\times10^{-3}$			5.65±3	-1.0±3	
White[54]			$(27\pm3)\times10^{-10}$	$(9.5\pm.6)\times10^{-11}$	1.5±.2		2.25±.2
Andres[53]			$(33\pm3)\times10^{-10}$	$(6.6\pm.6)\times10^{-11}$	1.8±.2		1.98±.2
This work	$(-2.7\pm.06)\times10^{-3}$	$(-4.0\pm.2)\times10^{-3}$			6.45±3	-2.3±3	

Notes:

(1) Values of $\frac{d\ln\gamma}{d\ln V}$ and Γ_G were calculated from thermal expansion data by using equations (42) and (43), and the following parameters: γ = 1.35 mj/mole $^oK^2$, θ_D = 427.7 ^oK (Phillips[68]), $K_n = 1.34 \times 10^{-6}$ atm^{-1} (Brandt and Ginzburg[49]), and V = 9.87 cm^3/mole.[71]

(2) Values of $\frac{d\ln\gamma}{d\ln V}$ from critical field results were calculated from equation (87), using H_o, T_c, and $\left(\frac{dH_c(T_c)}{dT}\right)_P$ from our zero pressure results, and using the compressibility value given above.

(3) Values of $\frac{d\ln A}{d\ln V}$ were calculated from (69).

It is interesting to compare our result for $\frac{d\ln\gamma}{d\ln V}$ with the result predicted by the free electron model. The free electron model predicts[85]

$$\gamma = \frac{\pi^2 kz}{2} R/E_f \tag{99}$$

where

z = no. of electrons/atom

R = gas constant

E_f = Fermi Energy $\propto \left(\frac{z}{V}\right)^{2/3}$

V = molar volume .

Hence

$$\gamma \propto V^{2/3} \tag{100}$$

and

$$\frac{d\ln\gamma}{d\ln V} = \frac{2}{3} \quad . \tag{101}$$

All values listed in Table 6, including our result, are considerably larger than this. This is not surprising in light of Melz's[86] DeHass-van Alphen effect measurements of the effect of pressure on the Fermi surface of aluminum. Melz found changes in the Fermi surface with pressure which were much larger than predicted by the nearly free electron model.

In the nearly free electron model, the electronic band structure is estimated by drawing the free-electron Fermi sphere corresponding to z electrons per atom about a reciprocal lattice point, and translating pieces of the Fermi sphere in higher Brillouin zones back into the first zone with reciprocal lattice vectors. The model thus represents a metal in the limit in which the lattice potential approaches zero, serving only to cause Bragg reflection.

According to the nearly free electron model, an isotropic compression of the lattice should not change the size or shape of the Fermi surface relative to the zone boundaries.[87] That is, as the lattice is compressed, the Fermi surface and Brillouin zones will expand such that all relative dimensions remain unchanged. However, the nearly free electron model does not take into account changes in band structure which accompany changes in interatomic spacing. Such band structure effects have little effect on the shape of the Fermi surface or on the density of states at the Fermi surface if the Fermi surface is well away from zone boundaries. However, if the Fermi surface is close to zone boundaries, the electron states near the Fermi level are no longer free-electron-like, due to Bragg reflection, and the lattice potential has a large effect on the spacing of the energy levels and on the shape of the Fermi surface.

Aluminum has three electrons per atom, and the Fermi surface is complicated and very close to zone boundaries.[87,88] It is reasonable to expect, then, that the density of states at the Fermi surface would be more sensitive to volume changes than is predicted by the free electron model.

REFERENCES

1. H. K. Onnes, Commun. Kamerlingh Onnes Lab. Univ. Leiden Suppl. 34b, 55 (1913).

2. D. Shoenberg, Superconductivity (Cambridge, London, 1958).

3. E. A. Lynton, Superconductivity (Wiley, New York, 1962).

4. W. Meissner and R. Ochsenfeld, Naturwissenschaften 21, 787 (1933).

5. D. Schoenberg, Superconductivity (Cambridge, London, 1958), Chapters 3 and 4.

6. B. S. Chandrasekhar and J. A. Rayne, Phys. Rev. Letters 6, 3 (1961).

7. G. A. Alers and D. L. Waldorf, IBM Journal 6, 89 (1962).

8. B. Serin, C. A. Reynolds, and L. B. Nesbitt, Phys. Rev. 80, 761 (1950).

9. Herzfeld, Maxwell, and Scott, Phys. Rev. 79, 911 (1950).

10. D. K. Finnemore and D. E. Mapother, Phys. Rev. Letters 9, 288 (1962).

11. T. H. Geballe, B. T. Matthias, G. W. Hull, Jr., and E. Corenzwit, Phys. Rev. Letters 6, 275 (1961).

12. J. W. Garland, Phys. Rev. Letters 11, 114 (1963).

13. B. B. Goodman, Proc. Phys. Soc. (London) A66, 217 (1953).

14. W. S. Corak, B. B. Goodman, C. B. Satterthwaite, and A. Wexler, Phys. Rev. 102, 656 (1956).

15. J. Bardeen, L. N. Cooper, and J. R. Schrieffer, Phys. Rev. 108, 1175 (1957).

16. D. H. Douglass, Jr. and L. M. Falicov, The Superconducting Energy Gap, in Progress in Low Temperature Physics, edited by C. J. Gorter. (North Holland Publishing Co., Amsterdam, 1961), Vol. IV.

17. See, for instance, Ref. 3, p. 77.

18. J. C. Swihart, D. J. Scalapino, and Y. Wada, Phys. Rev. Letters 14, 106 (1965).

19. D. K. Finnemore and D. E. Mapother, Phys. Rev. 140, A507 (1965).

20. C. A. Swenson, IBM Journal 6, 82 (1962).

21. D. E. Mapother, Phys. Rev. 126, 2021 (1962).

22. B. Mühlschlegel, Z. Physik 155, 313 (1959).

23. J. F. Cochran and D. E. Mapother, Phys. Rev. 121, 1688 (1961).

24. D. L. Decker, D. E. Mapother, and R. W. Shaw, Phys. Rev. 112, 1888 (1958).

25. J. G. Daunt and K. Mendelssohn, Proc. Roy. Soc. (London) A160, 127 (1937).

26. C. A. Shiffman, J. F. Cochran, and M. Garber, J. Phys. Chem. Solids 24, 1369 (1963).

27. B. J. C. van der Hoeven, Jr. and P. H. Keesom, Phys. Rev. 135, A631 (1964).

28. N. E. Phillips, M. H. Lambert, and W. R. Gardner, Rev. Mod. Phys. 36, 131 (1964).

29. C. H. Hinrichs and C. A. Swenson, Phys. Rev. 123, 1106 (1961).

30. R. W. Shaw, D. E. Mapother, and D. C. Hopkins, Phys. Rev. 120, 88 (1960).

31. D. White, C. Chou, and H. L. Johnston, Phys. Rev. 109, 797 (1958).

32. C. A. Bryant and P. H. Keesom, Phys. Rev. 123, 491 (1961).

33. H. R. O'Neal and N. E. Phillips, Phys. Rev. 137, A748 (1965).

34. W. R. Wilkes, Thesis, Univ. of Illinois (1966).

35. W. S. Corak and C. B. Satterthwaite, Phys. Rev. 102, 662 (1956).

36. J. R. Clement and E. H. Quinell, Phys. Rev. 92, 258 (1953).

37. M. Horowitz, A. A. Silvidi, S. F. Malaker, and J. G. Daunt, Phys. Rev. 88, 1182 (1952).

38. R. L. Dolecek, Phys. Rev. 94, 540 (1954).

39. D. C. Hopkins, Thesis, Univ. of Illinois (1962).

40. D. C. Rorer, H. Meyer, and R. C. Richardson, Z. Naturforschg. 18a, 130 (1963).

41. J. F. Cochran and D. E. Mapother, Phys. Rev. 111, 132 (1958).

42. S. Caplan and G. Chanin, Phys. Rev. 138, A1428 (1965).

43. D. E. Mapother (private communication).

44. See, for example, Ref. 2, Section 3.5.

45. D. P. Seraphim and P. M. Marcus, IBM Journal 6, 94 (1962).

46. P. Morel, J. Phys. Chem. Solids 10, 227 (1959).

47. J. L. Olsen and H. Rohrer, Helv. Phys. Acta 33, 872 (1960).

48. C. A. Swenson, in Solid State Physics (Academic Press, New York, 1960), edited by F. Seitz and D. Turnbull, Vol. II, p. 41.

49. N. B. Brandt and N. I. Ginzburg, Usp. Fiz. Nauk 85, 485 (1965) [English Translation: Soviet Physics Uspekhi 8, 202 (1965)].

50. J. L. Olsen, Helv. Phys. Acta 32, 310 (1959).

51. D. Gross and J. L. Olsen, Cryogenics 1, 91 (1960).

52. N. E. Alekseevskii and Y. P. Gaidukov, Zh. Eksperim. i Teor. Fiz. 30, 1058 (1956) [English Translation: Soviet Phys. - JETP 2, 762 (1956)].

53. K. Andres, Phil. Mag. 6, 815 (1961).

54. G. K. White, Cryogenics 2, 125 (1963).

55. J. E. Schirber and C. A. Swenson, Phys. Rev. 123, 1115(1961).

56. M. Garfinkel and D. E. Mapother, Phys. Rev. 122, 459 (1961).

57. P. W. Bridgman, The Physics of High Pressures (G. Bell, London, 1949).

58. R. I. Beecroft and C. A. Swenson, J. Appl. Phys. 30, 1793 (1959).

59. J. F. Cochran, D. E. Mapother, and R. E. Mould, Phys. Rev. 103, 1657 (1956).

60. L. Onsager, J. Am. Chem. Soc. 58, 1486 (1936).

61. M. H. Hebb and E. M. Purcell, J. Chem. Phys. 5, 338 (1937).

62. D. de Klerk and R. P. Hudson, Phys. Rev. 91, 278 (1953).

63. W. E. Gardner and N. Kurti, Proc. Phys. Soc. (London) A223, 542 (1954).

64. F. G. Brickwedde, H. van Dijk, M. Durieux, J. R. Clement, and J. K. Logan, J. Research Natl. Bur. Standards 64A, 1 (1960).

65. C. Blake, C. E. Chase, and E. Maxwell, Rev. Sci. Inst. 29, 715 (1958).

66. A. C. Anderson, Thesis, Univ. of Illinois (1961).

67. R. E. Harris, Technical Report #1, Prepared under Grant No. DA-ARO-343 (1966).

68. N. E. Phillips, Phys. Rev. 114, 676 (1959).

69. B. B. Goodman, Compt. Rend. 244, 2899 (1957).

70. N. V. Zavaritskii, Zh. Eksperim. i Teor. Fiz. 34, 1116(1958) [English Translation: Soviet Physics - JETP 7, 773 (1958)].

71. B. F. Figgins, G. O. Jones, and D. P. Riley, Phil. Mag. 1, 747 (1956).

72. Yardley Beers, Introduction to the Theory of Error (Addison-Wesley, Reading, Massachusetts, 1958), Chap. VI, Section B.

73. J. Clem, Thesis, Univ. of Illinois (1965).

74. B. B. Goodman and E. Mendoza, Phil. Mag. 42, 594 (1951).

75. T. E. Faber, Proc. Roy. Soc. (London), A231, 353 (1955).

76. M. A. Biondi, M. P. Garfunkel, and W. A. Thompson, Phys. Rev. 136, A1471 (1964).

77. M. A. Biondi and M. P. Garfunkel, Phys. Rev. 116, 853 (1959).

78. R. David and N. J. Poulis, Proceedings of the Eighth International Conference on Low Temperature Physics (Butterworths, London, 1963). p. 193.

79. N. V. Zavaritskii, Zh. Eksperim. i Teor. Fiz. 41, 657 (1961) [English Translation: Soviet Phys. - JETP 14, 470 (1962)].

80. D. Douglass, Jr. and R. Meservey, Proceedings of the Eighth International Conference on Low Temperature Physics (Butterworths, London, 1963), p. 180.

81. I. Giaever and K. Megerle, Phys. Rev. 122, 1101 (1961).

82. S. Shapiro, P. H. Smith, J. Nicol, J. L. Miles, and P. F. Strong, IBM Journal 6, 34 (1962).

83. Y. Masuda and A. Redfield, Phys. Rev. 125, 159 (1962).

84. N. L. Muench, Phys. Rev. 99, 1814 (1955).

85. C. Kittel, Introduction to Solid State Physics (Wiley, New York, 1959), p. 258.

86. P. Melz, Thesis, Univ. of Illinois (1966).

87. W. A. Harrison, Influence of Pressure on the Fermi Surface in Metals, in Physics of Solids at High Pressures, edited by C. Tomizuka and R. Emrick (Academic Press, New York, 1965).

88. W. A. Harrison, Psendopotentials in the Theory of Metals (W. A. Benjamin, New York, 1966), Chapter 3.

98. D. Markowitz and L. P. Kadanoff, Phys. Rev. 131, 563 (1963).

90. G. Chanin, E. A. Lynton, and B. Serin, Phys. Rev. 114, 719 (1959).

91. J. P. Franck and D. L. Martin, Can. J. Phys. 39. 1320 (1961).

92. J. F. Cochran, C. A. Shiffman, and J. E. Neighbor, Rev. Sci. Instr. 37, 499 (1966).

93. B. J. C. van der Hoeven, Jr. and P. H. Keesom, Phys. Letters, 3, 360 (1963).

Appendix A

DISCUSSION OF EXPERIMENTAL UNCERTAINTIES

1. Uncertainties in Temperature Measurement

Estimates of the uncertainty in the temperature measurements are given in Table 7. Of interest for calculation of the pressure dependence of the critical field data are the relative uncertainties between temperature measurements made at different pressures and during the two different runs. Such uncertainties might arise from the following sources:

(i) Uncertainties and shifts in the resistor calibrations

(ii) Scatter in the raw mutual inductance data of run 2 for $T < 0.8^{o}K$

(iii) Inconsistencies in temperature measurement between runs 1 and 2 due to errors in salt pill calibration.

The uncertainty due to (iii) can be estimated by comparing the zero pressure critical field data from runs 1 and 2. Making this comparison, we find (see Figure 10, Chapter III) agreement within experimental error ignoring any possible uncertainty due to (iii). Thus, in estimating relative uncertainties in the temperature measurements we consider only the contributions from (i) and (ii).

Table 7

UNCERTAINTIES IN TEMPERATURE MEASUREMENTS
AT REPRESENTATIVE TEMPERATURES

Source of Error	Uncertainty (^{o}K)		
	T=1^{o}K	T=.7^{o}K	T=.3^{o}K
Salt Pill Calibration	±.0007	±.0007	±.0004
T - T* Relations	±.001	±.002	±.002
Relative uncertainty due to errors in resistor calibration or salt pill measurement	±.0006	±.0005	±.0001
Limit of Error(Absolute)	±.0023	±.0032	±.0025
Limit of Error(Relative)	±.0006	±.0005	±.0001

2. Uncertainties in Critical Field Measurement

Estimates of the absolute and relative uncertainties in the critical field measurements are summarized in Table 8.

Table 8

UNCERTAINTIES IN CRITICAL FIELD MEASUREMENT

Source	Absolute Uncertainty (gauss)	Relative Uncertainty (gauss)
Solenoid calibration	$\pm.0002\ H_c$	
Field inhomogeneity	$\pm.0003\ H_c$	
Incomplete cancellation of stray fields	$\pm.04$ gauss	$\pm.01$ gauss
Graphical determination of H_c from permeability plot	$\pm.02$ gauss $\pm.0004\ H_c$	$\pm.02$ gauss $\pm.0004\ H_c$
Uncertainty in positioning sample in solenoids	$\pm.0001\ H_c$	
Limits of Error	$\pm.06$ gauss $\pm.001\ H_c$	$\pm.03$ gauss $\pm.0004\ H_c$

Appendix B

CRITICAL FIELD DATA

Table 9

ZERO PRESSURE CRITICAL FIELD DATA

H_c (gauss)	T(^{o}K)	H_c (gauss)	T(^{o}K)
96.95	.3082	61.88	.7175
96.58	.3142	61.95	.7179
96.25	.3207	54.58	.7810
95.80	.3276	44.85	.8600
95.28	.3372	44.76	.8603
95.85	.3430	40.87	.8914
94.66	.3477	36.37	.9259
94.00	.3593	36.09	.9264
93.49	.3654	31.09	.9656
93.11	.3724	28.52	.9845
92.17	.3870	28.17	.9852
92.21	.3871	25.48	1.0062
91.09	.4038	23.50	1.0183
91.01	.4038	22.23	1.0291
89.69	.4226	18.78	1.0533
88.87	.4339	18.49	1.0543
88.06	.4445	16.60	1.0685
85.95	.4711	14.74	1.0801
85.88	.4717	14.32	1.0843
83.43	.5028	11.89	1.1006
83.29	.5028	10.69	1.1074
80.13	.5408	9.36	1.1176
79.86	.5415	6.66	1.1352
75.41	.5890	6.48	1.1366
75.37	.5910	3.95	1.1535
71.92	.6256	1.76	1.1676
67.46	.6669	1.01	1.1726
67.42	.6672		

Table 10

3100 psi CRITICAL FIELD DATA

H_c (gauss)	T(^oK)	H_c (gauss)	T(^oK)
96.37	.3056	66.79	.6671
96.07	.3120	61.18	.7181
95.67	.3188	53.85	.7814
95.24	.3259	44.08	.8602
94.76	.3354	40.00	.8916
94.12	.3459	35.46	.9262
93.40	.3577	30.04	.9659
92.59	.3707	27.69	.9848
91.63	.3855	24.62	1.0065
90.50	.4022	21.34	1.0295
89.12	.4214	17.83	1.0537
87.50	.4438	15.65	1.0687
86.73	.4537	13.53	1.0847
85.48	.4700	10.92	1.1011
82.81	.5014	8.46	1.1181
79.36	.5409	5.73	1.1357
74.72	.5893	2.91	1.1540
71.20	.6248	1.01	1.1666

Table 11

5400 psi CRITICAL FIELD DATA

H_c (gauss)	T(^oK)	H_c (gauss)	T(^oK)
96.81	.2905	74.12	.5903
96.30	.3000	66.20	.6671
95.87	.3087	60.65	.7176
95.33	.3181	53.33	.7811
94.87	.3268	43.52	.8603
94.30	.3365	34.93	.9264
93.69	.3471	27.08	.9854
92.52	.3653	22.49	1.0183
91.16	.3869	17.27	1.0543
89.99	.4036	13.51	1.0801
87.82	.4334	9.45	1.1074
84.94	.4715	5.09	1.1366
82.19	.5026	1.36	1.1613
78.88	.5415		

Table 12

7200 psi CRITICAL FIELD DATA

H_c (gauss)	T(^{o}K)	H_c (gauss)	T(^{o}K)
95.06	.3166	65.79	.6671
94.46	.3257	60.19	.7180
93.92	.3358	52.90	.7810
93.26	.3471	43.01	.8603
92.14	.3654	34.40	.9264
90.69	.3870	26.30	.9852
89.54	.4037	21.78	1.0183
87.35	.4337	16.74	1.0543
84.41	.4717	12.94	1.0801
81.85	.5025	8.82	1.1074
78.41	.5417	4.51	1.1366
73.76	.5901	1.66	1.1550

VITA

Erik Preston Harris was born on December 16, 1938 in Columbus, Ohio. He received his elementary and secondary education in the Columbus public school system. He attended Cornell University, receiving the degree of Bachelor of Engineering Physics in June, 1961. Since that time, he has been a graduate student at the University of Illinois, from which he received a Master of Science degree in February, 1963. He is a member of the American Physical Society.

Unclassified
Security Classification

DOCUMENT CONTROL DATA - R&D

(Security classification of title, body of abstract and indexing annotation must be entered when the overall report is classified)

1. ORIGINATING ACTIVITY (Corporate author)	2a. REPORT SECURITY CLASSIFICATION
University of Illinois	Unclassified
	2b GROUP: NA

3 REPORT TITLE

CRITICAL FIELD OF SUPERCONDUCTING ALUMINUM AS A FUNCTION OF PRESSURE AND TEMPERATURE ABOVE 0.3°K

4 DESCRIPTIVE NOTES (Type of report and inclusive dates)

Technical Report

5 AUTHOR(S) (Last name, first name, initial)

Harris, Erik T.

6 REPORT DATE	7a TOTAL NO. OF PAGES	7b. NO OF REFS
November 1966	106	23

8a CONTRACT OR GRANT NO.	9a ORIGINATOR'S REPORT NUMBER(S)
DA-31-124-ARO(D)-357	None
b. PROJECT NO. 20014501B11B	
c.	9b OTHER REPORT NO(S) (Any other numbers that may be assigned this report)
d.	2771.13

10. AVAILABILITY/LIMITATION NOTICES

Distribution of this report is unlimited.

11. SUPPLEMENTARY NOTES	12. SPONSORING MILITARY ACTIVITY
None	U.S. Army Research Office-Durham Box CM, Duke Station Durham, North Carolina 27706

13 ABSTRACT The critical field curve of aluminum has been measured from T_c to 0.3°K, at pressures ranging from 0 to 7200 psi. Using calorimetrically derived values for the low-temperature superconducting electronic specific heat, the data have been extrapolated to T = 0, yielding values for H_o and γ. These values and experimental results for T_c are then used to calculate the superconducting electronic entropy and the deviation of the critical field curve from parabolicity over the entire temperature range. The results show excellent agreement with previous calorimetric measurements of the thermodynamic properties of superconducting aluminum. The shape of the reduced critical field curve shows no pressure dependence over the range of pressures used. The dependence of H_o, T_c, and γ on pressure are in fair agreement with previous work by Gross and Olsen.

14. KEY WORDS

Aluminum
Critical Field
Low-Temperature
Superconductors
Specific Heat
Superconducting Electronic Entropy
Thermodynamic Properties
Pressure Dependence

DD FORM 1 JAN 64 1473

Unclassified
Security Classification